University of Leoben

Diploma Thesis

The influence of high current densities on intact and cracked thin gold films on flexible polyimide substrate

Barbara Putz

Leoben, May 2014

This work was carried out at the Erich Schmid Institute of Material Science with support for research provided by the Austrian Science Foundation (FWF) through project P22648-N20.

University of Leoben
Franz Josef Straße 18
8700 Leoben
Austria

Erich Schmid Institute of Material Science
Austrian Academy of Sciences
Jahnstraße 12
8700 Leoben
Austria

EIDESSTATTLICHE ERKLÄRUNG

Ich erkläre an Eides statt, dass ich diese Arbeit selbständig verfasst, andere als die angegebenen Quellen und Hilfsmittel nicht benutzt und mich auch sonst keiner unerlaubten Hilfsmittel bedient habe.

DECLARATION OF AUTHORSHIP

„I declare in lieu of oath that this thesis is entirely my own work except where otherwise indicated. The presence of quoted or paraphrased material has been clearly signalled and all sources have been referred. The thesis has not been submitted for a degree at any other institution and has not been published yet."

Leoben, May 2014

____

(Barbara Putz)

i Danksagung

An dieser Stelle möchte ich mich bei allen Personen bedanken, die mich bei der Erstellung dieser Arbeit und während meines Studiums unterstützt haben.

Mein besonderer Dank gilt Frau Dr. Megan Cordill für die interessante und anspruchsvolle Aufgabenstellung meiner Diplomarbeit, die motivierende Betreuung und die zahlreichen Anregungen und Ideen die zur erfolgreichen Umsetzung der Arbeit beigetragen haben.

Bei Dr. Oleksandr Glushko möchte ich mich bedanken, für die Unterstützung bei meinen Experimenten und bei der Interpretation der teilweise abenteuerlichen Ergebnisse.

Mein Dank geht auch an Dr. Thomas Schöberl ohne dessen Erfahrung und Unterstützung viele AFM Aufnahmen um einiges länger gedauert hätten.

Mein Dank für die organisatorische Hilfe geht an Viktoria Schrutt und Maria Anna Fließer.

Weiters möchte ich mich bei meinen Kollegen am Institut bedanken, für das freundliche Arbeitsklima, gute Ratschläge und aufmunternde Worte wenn einmal etwas schief ging. Ebenso bei meinen Freunden und Studienkollegen, die diese Arbeit korrigiert haben und durch ihre Freundschaft die Zeit in Leoben unvergesslich gemacht haben.

Ein besonders großer Dank gilt meinen Eltern und meiner Familie, für die finanzielle Unterstützung, Rückhalt und das Gefühl alles schaffen zu können. Danke Peter, für die künstlerische Gestaltung der Arbeit, deine Geduld und deine Unterstützung während und abseits des Studiums.

ii Abstract

Thin metal films on compliant polymer substrates are of major interest for their use in flexible electronics, for applications as diverse as rollable displays or artificial skin. The operating current densities of today's flexible electronic devices are low in the range of µA – mA/cm², but smaller and more powerful devices demand for higher current densities in future flexible electronics making electromigration, a current driven self-diffusion of metal atoms, a major reliability concern. This work investigates the effect of high current densities on intact and cracked gold thin films on a polyimide substrate and the possible occurrence of electromigration. Through thickness cracks perpendicular to the straining direction are introduced into 50 nm Au films with a 10 nm Cr interlayer by uniaxial straining. The cracking behaviour is investigated mechanically and electrically with fragmentation testing and in-situ 4 point probe resistance measurements, respectively. The Cr interlayer causes brittle behaviour of a normally ductile Au film. Artificial single cracks are generated in 50 nm gold films with and without Cr interlayer. Both sample configurations are subjected to various current densities over different time frames while the electrical resistance of the film is recorded. The electrical stability and the possible occurrence of electromigration are detected by measuring the variation of the electrical resistance of the film as well as by imaging of the sample surface before and after electrical treatment using scanning electron microscopy. Atomic force microscopy and energy dispersive X-ray analysis of different phenomena obtained during testing indicate the occurrence of electromigration. Finally, measures to improve electromigration testing of thin films on flexible polymer substrates are recommended.

iii Kurzfassung

Dünne Metallfilme auf flexiblen Polymersubstraten sind von großem Interesse für Technik und Wirtschaft aufgrund ihrer Verwendung als Leitermaterial in flexibler Elektronik. Der Anwendungsbereich dieser neuen, vielversprechenden Technologie reicht von aufrollbaren Bildschirmen bis hin zu künstlichen Hautimplantaten. Die Betriebsstromdichten heutiger Bauteile liegen im Bereich von µA bis mA/cm². Der Trend hin zu kleineren, leistungsstärkeren Bauteilen erfordert höhere Betriebsstromdichten in der flexiblen Elektronik der Zukunft und macht dadurch Elektromigration zu einem ernstzunehmenden Zuverlässigkeitskriterium. Diese Arbeit untersucht den Einfluss hoher Stromdichten auf intakte und rissbehaftete dünne Goldfilme auf einem flexiblen Polyimid-Substrat und das mögliche Auftreten von Elektromigration. Durch einachsiges Ziehen werden Risse in 50 nm dicken Goldfilmen mit einer 10 nm dicken Chrom-Zwischenschicht generiert. Die Rissentwicklung wird mechanisch mittels Fragmentierungs-Test und elektrisch mittels in-situ 4-Punkt-Widerstandsmessungen untersucht. Die 10 nm Chrom-Zwischenschicht verursacht sprödes Verhalten der sonst duktilen Goldschicht. Künstliche Einzelrisse werden in 50 nm Goldfilmen mit und ohne Chrom-Zwischenschicht generiert. Um die elektrische Stabilität und das mögliche Auftreten von Elektromigrationseffekten zu untersuchen werden beide Probenkonfigurationen unterschiedlichen Stromdichten über unterschiedlich lange Zeiträume ausgesetzt. Während der elektrischen Belastung wird der Widerstand der Metallschicht aufgezeichnet. Die Veränderung des Widerstandes während sowie optische Untersuchungen der Probenoberfläche nach der elektrischen Belastung geben Aufschluss über mikrostrukturelle Veränderungen. Rasterkraftmikroskopische Untersuchungen und energiedispersive Röntgenanalyse von Phänomenen, die durch die elektrische Behandlung erzielt wurden, deuten auf das Auftreten von Elektromigration hin. Abschließend werden Maßnahmen zur Veränderung der elektrischen Testmethode vorgeschlagen um die Elektromigrationsprüfung dünner Metallschichten auf flexiblen Polymersubstraten zu verbessern.

Contents

i Danksagung -i-

ii Abstract -ii-

iii Kurzfassung -iii-

1 Introduction – Flexible Electronics - 1 -

2 Literature overview - 3 -

2.1 Thin film deposition - 3 -

2.1.1 Thermal evaporation - 3 -

2.1.2 Sputtering - 4 -

2.2 Mechanical properties of thin metal films on flexible polymer substrate - 5 -

2.2.1 Ductile films - 6 -

2.2.2 Brittle films - 7 -

2.2.3 Fragmentation test for brittle and ductile metal films - 8 -

2.3 Electromechanical properties of thin metal films on flexible polymer substrate - 10 -

2.3.1 In-situ 4 Point Probe measurement [6] - 11 -

2.4 Electrical properties of thin metal films on polymer substrate - 13 -

2.4.1 Electrical testing - 14 -

2.5 Electromigration - 15 -

2.5.1 Drift test - 16 -

2.5.2 Electromigration lifetime extrapolation, Black Law - 19 -

3 Experimental - 20 -

3.1 Starting material - 20 -

3.2 Material characterisation - 21 -

3.3 Fragmentation testing - 22 -

3.4 Electro-mechanical testing – In-situ 4 Point Probe measurement - 22 -

3.5 Electrical testing .... - 23 -

4 Results and Discussion .... - 25 -

4.1 Fragmentation test .... - 25 -

4.2 In-situ 4PP experiment .... - 27 -

4.3 Electrical testing .... - 30 -

4.3.1 Electromigration .... - 39 -

5 Summary and Outlook .... - 46 -

5.1 Electro-mechanical properties of Au and AuCr on PI .... - 46 -

5.2 Electrical stability of Au and AuCr on PI; Electromigration .... - 47 -

I List of abbreviations - I -

II List of figures - IV -

III List of tables - VIII -

IV References - IX -

1 Introduction – Flexible Electronics

By adding flexibility to conventional rigid electronics a whole field of new and promising possibilities opens up. Flexible electronic applications can be as diverse as paper-like rollable displays (e-paper), smart wearable electronic clothing, smart artificial skin, electronic eyes or implantable medical devices [1, 2]. Cheap, robust and reliable flexible lightweight electronics that are easily portable are required to realize the above mentioned applications.

To fulfil all these requirements the devices consist of different layers of thin films made of various materials such as metals, semiconductors and ceramics placed on flexible polymer substrates. Thin metallic films on flexible polymer substrates are of great scientific and industrial interest for their use in flexible electronic devices and their performance was excessively investigated during the last decades [2]. Metallic films constitute the electric circuits in flexible electronic devices [2].Copper and gold are favourable metals to use because of their good ductility and excellent conductive properties. Additionally, much is known about depositing these materials onto rigid substrates [3]. Gold, investigated in this work, is particularly suitable as a conductive layer due to its low resistivity, high thermal stability and good oxidation stability and chemical inertness. Other materials used for the electric circuits include silver inks, ITO (indium tin oxide) films or conducting polymers such as Poly (3,4-ethylenedioxythiophene) poly (styrenesulfonate) (PE DOT:PSS).The latter two are optical transparent conductors used in optical devices.

The polymer substrate primary supports the device and offers the required flexibility, compared to conventional rigid ceramic or glass substrates. Contrary to ceramic or glass substrates the thermal stability of polymers is rather low. Commonly used substrates include polyesters (PE), polyethylene terephthate (PET), polycarbonate (PC) or polyimide (PI). The latter serves as substrate for the investigated gold films in this thesis. Its greatest advantages are a relatively high temperature stability ($T_S \sim 400$ °C) and stability against weather [3].

The usability of a flexible electronic device stands and falls with the electro-mechanical performance of the metal film/polymer substrate couple. Therefore, it is essential to assess the mechanical and electrical properties of the film and substrate together. The "stretchability" of a film/substrate system is the ability to support large stretching, compressing, bending and twisting distortions in use, without failing mechanically or electrically. In

order to get a high stretchability range a high fracture strain and good adhesion between the film and the substrate are required. For the electrical performance a high charge carrier mobility at high strains is desirable [3]. In this work, among other things, the mechanical and electrical behaviour of a gold/polyimide couple with and without Cr interlayer are investigated.

The current densities in today's flexible electronics are generally low in the range of µA-mA/cm². For future applications it is important to investigate the influence of high current densities on the performance of metal film/flexible substrate systems. Smaller and more powerful devices demand higher current densities in use. Furthermore, long term performance at low current densities can be predicted by extrapolating data obtained from short term experiments at higher current densities. Several effects need to be taken into account while operating with high current densities. Electromigration typically occurs at current densities > 1 MA/cm² [4] in metallic conductors and can cause the loss of current carrying capability or electrical shortcuts. Thin films are especially prone to electromigration effects. Their microstructure is composed of a large number of rapid low-temperature diffusion paths, such as grain boundaries and interfaces, that allows significant mass transport [5]. Furthermore, local melting of the polymer substrate due to temperature increase and Joule Heating can lead to failure of the device. Of special interest is the influence of cracks present in the conductive metallic layer on its performance at high current densities. Such cracks can be easily generated during stretching of the device and prolong or more likely shorten the lifetime of the application.

This work discusses problems arising from high current densities in flexible electronics. It investigates the influence of high current densities on intact and cracked thin gold films on polyimide and provides explanations for interesting potential electromigration phenomena that occurred during electrical testing. Finally, suggestions on how to improve electromigration testing for thin metal films on flexible polymer substrates are covered at the end.

2 Literature overview

2.1 Thin film deposition

The development of fabrication technologies allowing for cost-effective, fast, easy and reliable production of large-area integrated circuits is one of the main challenges on the way to mass production of flexible electronics. Thin metal films must be deposited on flexible substrates to fabricate thin film transistors, active elements and metal interconnections etc. [6].In order to get good electrical and mechanical properties during flexing and stretching the film/polymer structures need to fulfil several requirements. Good adhesion at the metal-polymer interface, uniform microstructure and film thickness, absence of voids and impurities, a low defect density and a low electrical resistance are for example characteristics required for good electromechanical behaviour. The fabrication technology strongly influences these parameters, especially the adhesion, and therefore, determines whether a thin metal film is suitable for metallization in integrated circuits.

For research applications conventional thin film deposition techniques such as sputtering or thermal evaporation are used to create flexible electronics [3]. Therefore a short description of the two techniques mentioned above will be provided including their major advantages and disadvantages. Both techniques belong to the category of physical vapour deposition (PVD). The Au films investigated in this work are sputter deposited.

2.1.1 Thermal evaporation

The principle of thermal evaporation is that a metal, which is to be deposited in order to form the thin film, is evaporated from a source using thermal energy only. The vaporised atoms in turn condense on the substrate surface forming the film. The process takes place in an evacuated chamber to prevent surface contamination. Figure 1 shows a schematic of thermal evaporation.

Parameters that influence the film properties are the temperature of the substrate, the evaporation rate and the pressure of the vacuum [7]. High deposition rates can be obtained with the drawback that homogeneous deposition and composition control are rather difficult. Compared to other deposition techniques, the adhesion to the polymer substrate is rather

poor [8]. The formation of bonds between metal atoms and the polymer substrate is responsible for adhesion and depends on the energy of the deposited metal atoms.

Thermal evaporation produces low energy vaporized atoms, with an energy range between 0.1 and 0.5 eV, which condense onto the sample surface. The heat liberated during condensation is only high enough to allow reaction between highly reactive metals and the polymer. Therefore, the process is not suitable for inert metals such as gold, since in order to get good adhesion between the metal and the polymer, metal-polymer bonds must be formed [9].

2.1.2 Sputtering

During sputtering atoms are ejected from a metal target through collisions with incident plasma-ions and deposited on a substrate surface. An electric field is imposed upon the metal target (cathode) and the substrate (anode). In between the anode and cathode an Argon plasma is located. Again vacuum is used to avoid contamination. The applied electric field causes the ionisation of the gas atoms and acceleration of the ions toward the target. As the ions hit the target, neutral metal-target atoms are ejected from the target-surface and deposited on the substrate. Threshold energy for the release of an atom from the target exists (binding energy), which needs to be exceeded by the kinetic energy of the incident ions. Otherwise the atom is not sputtered. Figure 2 shows a schematic of the sputter-process.

Sputter-deposited metal atoms have significantly higher energies than evaporated ones, which results in more extensive interfacial bonding between metal and polymer. The substantially increased adhesion obtained with sputter-deposition justifies the growing importance of metal sputtering as a deposition technique for thin metal films on polymers. Damaging effects due to substrate heating during sputtering can be minimized using low deposition rates [9]. The high kinetic energy of the sputtered atoms also leads to greater defect nucleation. The concentration of impurities in sputter-deposited films is generally higher than in films deposited by evaporation, due to the sputtering gas and lower vacuum pressure. The grain size of sputtered films is typically smaller than that of evaporated ones [10].

Sputtering has no limitations concerning the deposited materials and offers a better control of composition and uniform film thickness than evaporation deposition does. Several

different methods are used for the deposition of thin films in practical applications such as dc sputtering, radio frequency sputtering, magnetron sputtering and bias sputtering [10].

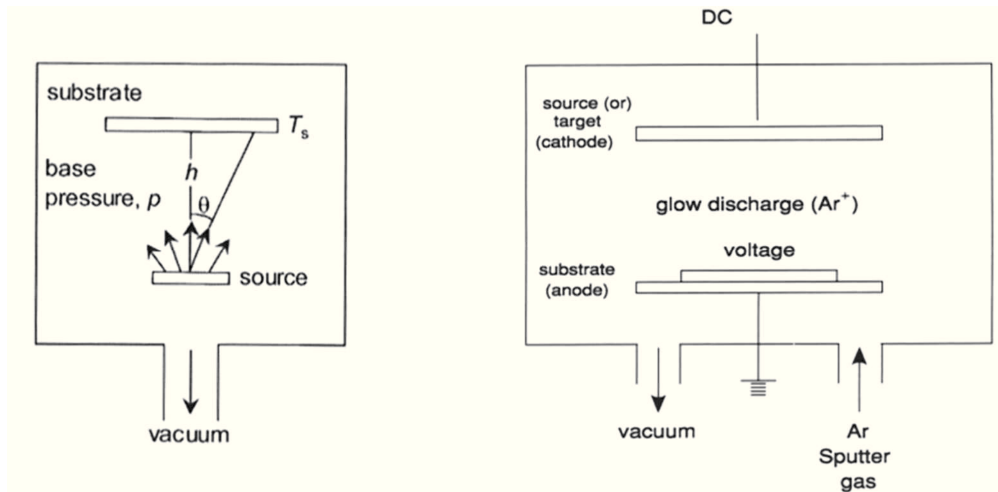

***Figure 1**: Schematic of an evaporation process. The metal, which is to be deposited, is evaporated from a source using thermal energy and condenses on the substrate surface forming a film [10].*

***Figure 2**: Schematic of a sputter process. Atoms are ejected from a metal target through collisions with incident plasma-ions and deposited onto a substrate surface forming a film [10].*

2.2 Mechanical properties of thin metal films on flexible polymer substrate

The deformation mechanisms of metal films on polymer substrates are comparable to those of free-standing films, but there are influences of the substrate and the interface on the film properties that need to be taken into account. Therefore, it is essential that the mechanical behaviour of the film and substrate is examined together and interfacial properties are investigated. In general, films on polymer substrates are easier to handle than free standing ones. Common techniques to measure the mechanical behaviour of thin films on rigid substrates, such as nanoindentation, are not suitable for films on compliant polymer substrates. Flexible film/substrate composites are mechanically tested using uniaxial tensile straining and fragmentation analysis. Testing can be performed in-situ using scanning electron microscopy (SEM), atomic force microscopy (AFM) or X-ray diffraction (XRD) to easily determine fracture strains [3]. An in depth description of fragmentation testing will be given in Chapter 2.2.3.

For the use in flexible electronics it is important that the film and the polymer can stretch and compress without mechanical or electrical failure [3]. Mechanical failure can be

plastic deformation, the formation of cracks or delamination and does not necessarily imply electrical failure. In any case, a transformation of the surface is induced, such as the formation of necks, cracks or buckles. The deformation mechanisms differ for brittle and ductile metal films and will be explained in more detail later. Film thickness and grain size can also influence the mechanical behaviour.

The polymer substrate influences the mechanical behaviour of the compound more than the film does. Its basic mechanical function is to support the metal film and increase the yield strength. By depositing a film on a pre-strained substrate compressive residual stresses can be introduced into the film, allowing for more tensile strain [3]. The roughness of an elastomeric substrate also influences the mechanical behaviour of the film. With very rough substrates a non-percolating crack pattern can develop in ductile thin films during straining [2].

Compared to bulk material the fracture strain of films on polymers are relatively small, but they can have high strengths. The reason for that is that localized deformation in the film is suppressed by the substrate, as long as the film remains bonded to the substrate and no delamination takes place [3].

2.2.1 Ductile films

A ductile, free-standing film under uniaxial tension ruptures due to strain localisation. During straining necking is obtained meaning that the film thins preferentially at a local spot by forming a neck perpendicular to straining direction. Further plastic deformation is then localised in this neck leading to rupture (progressive local thinning). The requirement for progressive local thinning is local elongation. The free standing film accommodates the local elongation as the ruptured halves move apart [11]. Rupture of a free-standing film can be seen in Figure 3 (a).

In ductile films, such as Au, Ag or Cu on a polymer substrate, also necking occurs when they are strained beyond the yield point. At small strains the substrate however can suppress the following strain localisation by constraining the local elongation needed for progressive local thinning. It delocalizes deformation in the metal film, enabling the film to become strained far beyond its necking limit without rupture. Only at higher strains fracture

occurs as the thinned regions (necks) transform into Through Thickness Cracks (TTCs), cracks that propagate through the whole film thickness. As a result, high fracture strains compared to free standing films can be obtained [12]. This effect is only present as long as the film is well bonded to the substrate. Once the film delaminates, it can be considered free standing, necking and failing [3]. Figure 3 (b) and (c) show the above mentioned behaviour of a substrate supported film and the case of delamination schematically.

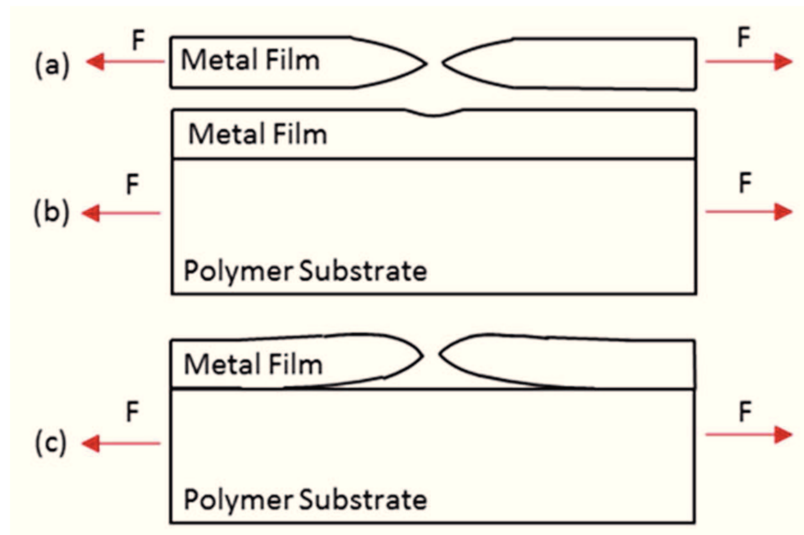

***Figure 3**: Failure of a ductile metal film, (a) free-standing and (b) on polymer substrate, (c) delamination [3].*

Adhesion between film and substrate is believed to be an important parameter influencing the fracture strain. Increasing adhesion leads to increasing fracture strain for the above mentioned effect [3].With increasing interface strength, three different types of tensile behaviour can be observed in the film, namely single-necking, multiple-necking and uniform deformation without the formation of necks [11].The adhesion of a metal-substrate system can be increased by adding an ultra-thin interlayer between the film and the substrate, with better adhesive properties. For ductile gold films it is common practise to use 10-30 nm of brittle Cr, W, Ti or Ta as interlayers [3, 13].

2.2.2 Brittle films

In brittle films fracture is caused by cleavage, which is breaking a single array of atomic bonds. No large local elongation occurs that could be suppressed by the substrate. That is

why the substrate does little to prevent the film from failure [3]. Brittle films fracture almost immediately when they are strained in tension, forming TTCs perpendicular to the straining direction [3]. Figure 4 shows the failure of a brittle film, free standing and on polymer substrate, schematically. The number of cracks increases with increasing strain until a certain saturation level is reached. After saturation the crack density remains constant with further increasing strain. The minimum distance between the cracks (crack spacing λ) at saturation is called saturation spacing λ_S. Saturation is due to the fact, that tensile stress is transferred from the substrate to the film via shear stress at the interface. This transfer requires a certain interfacial length. The length required to load the film with its fracture stress equals the saturation crack spacing. Below that length, the transferred stresses are too low and no further fracture occurs [14].

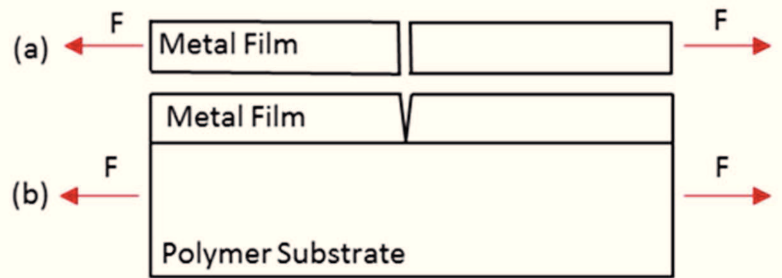

***Figure 4**: Failure of a brittle film, (a) free standing and (b) on polymer substrate [12].*

2.2.3 Fragmentation test for brittle and ductile metal films

Fragmentation testing is a relatively simple technique to assess the interface quality in thin film/compliant substrate systems. The method originates from fibre composite materials and has been modified to apply to film/substrate interfaces [3, 12, 15, 16]. It involves a uniaxial tensile test and a surface imaging technique and is, with slight changes, suitable for both brittle as well as ductile films. The basic principle is to analyse the deformation behaviour of the metal film obtained during uniaxial straining and thereby calculate interfacial properties. Several parameters, such as temperature, strain rate, film thickness and film thickness variation need to be taken into account, since they influence the deformation behaviour and therefore the calculated interfacial properties [17, 18].

A uniaxial tensile test is performed on a film/polymer composite. The stiff film deforms and fractures at lower strains than the compliant substrate. It has been mentioned before, that brittle films such as Ti, Cr or Ta form TTCs perpendicular to the straining direction.

The number of cracks increases with increasing strain until a saturation level is reached, where the distance between the cracks (crack spacing) reaches a minimum and remains constant (saturation spacing). Theory predicts, that in the saturation regime the longest spacing between two cracks is twice as large as the smallest [14]. One should note that the saturation crack spacing, λ_s, is not a single value but a statistical quantity.

The average crack spacing at different strains can be measured using an optical microscope, AFM or SEM and plotted over the applied strain as shown in Figure 5. The plateau indicates that the saturation spacing has been reached. Based on the crack density at saturation the interfacial shear strength between film and substrate can be evaluated using the following equation:

$$\tau_{max} = K * \frac{\delta * \sigma_f}{\lambda_s}, \quad (1)$$

where τ_{max} is the maximum shear stress sustained at the interface, δ is the film thickness, σ_f is the failure stress of the film, λ_s is the saturation crack spacing and K is a numerical constant [17].

In ductile films, such as Au, Ag or Cu, local thinning (necking) occurs when they are uniaxially strained beyond the yield point. Only at higher strains, these thinned regions transform into TTCs. Detecting and determining the necks with optical microscopy or SEM is difficult. To differentiate between necks and TTCs, a quantitative surface imaging technique, such as AFM, is needed. By measuring the film thickness δ and the depth of a certain deformation Δ, a Δ/δ ratio can be calculated and compared to a limit value, for example 15 %. If the calculated ratio exceeds this limit, it is considered a crack, otherwise the deformation in question is a neck. That way, a neck- a crack- and a deformation spacing can be determined. The deformation spacing is defined as the distance between necks and TTCs. It decreases with increasing strain and saturates above a certain strain limit, similar to the behaviour of brittle films (Figure 6) [19]. To fully understand the mechanical behaviour of ductile films it is important to distinguish between neck-, crack- and deformation spacing.

Uniaxial straining also induces compressive stresses in the film transverse to the straining direction, due to a mismatch in the Poisson's ratio between film and substrate. That is what can cause the film to buckle between the cracks and delaminate from the substrate. Buckling occurs at sufficiently high strains after saturation crack density has been reached and both materials (film and substrate) are in the plastic regime [20]. The observation of the

buckling pattern and delamination process with AFM can be used to determine interfacial characteristics such as adhesion energy [19, 21, 22]. In order to get good statistics, multiple images from different areas of the film need to be analysed. If the film has a very rough or damaged surface, imaging with the above mentioned techniques can be very hard or even impossible [19].

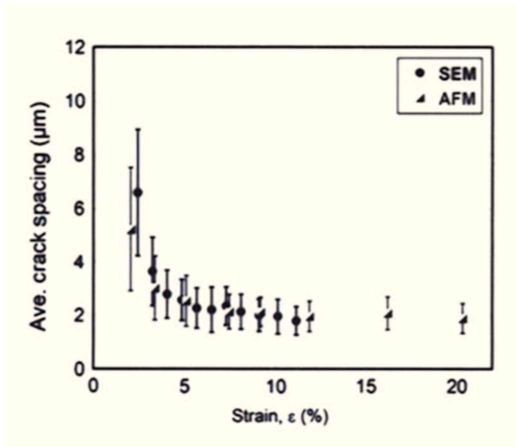

Figure 5: *Fragmentation Test of a brittle metal film. The average crack spacing measured with AFM and SEM is plotted over the applied strain. The plateau indicates saturation. SEM and AFM results follow one another closely [19].*

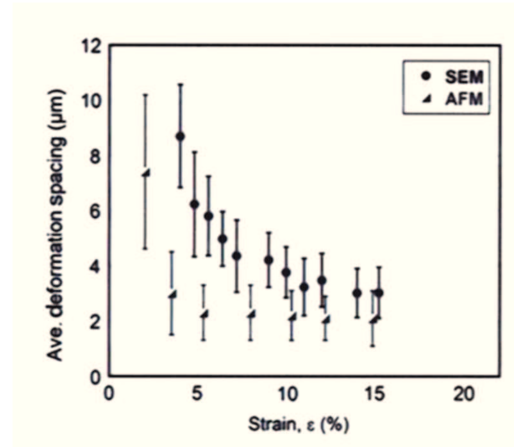

Figure 6: *Fragmentation Test of a ductile metal film. The average deformation spacing measured with AFM and SEM is plotted over the applied strain. The plateau indicates saturation. SEM and AFM results differ from each other, especially at small applied strains [19].*

2.3 Electromechanical properties of thin metal films on flexible polymer substrate

The electrical resistance of thin metal films on flexible polymer substrates is altered with mechanical straining of the film/substrate couple. As mentioned before, it is of major importance for the usability of flexible electronic devices that the film/polymer system does not fail electrically during mechanical stress, like bending or stretching in use. The "stretchability" of a metal film/ polymer substrate system is the ability to support large stretching, compressing, bending and twisting distortions, without failing mechanically or electrically. Stretching metallic conductors to large deformations while maintaining a low and constant electrical resistance is one of the main challenges in flexible electronics technologies [2, 23]. The roughness of an elastomeric substrate, among other things, influences the stretchability of a film/substrate couple. Literature reports that by depositing thin gold films onto rough

polydimethylsiloxane substrates, giant stretchabilities with deformations up to 100 % can be obtained while maintaining electrical conductivity [2].

2.3.1 In-situ 4 Point Probe measurement [6]

To determine the electromechanical behaviour of a film-substrate composite, a 4 point probe (4PP) resistance measurement incorporated into tensile straining grips is used for in-situ resistance measurements. While the sample is loaded and unloaded, the electrical resistance of the film is measured. Since the electrical contacts are integrated in the straining grips, only the electrical behaviour of the strained part of the sample is measured. Figure 7 show exemplary stress-strain and the corresponding R/R_0 curves derived from an in-situ 4PP resistance measurement. The actual shape of the graph depends on the tested film/substrate couple.

The initial resistance R_0 of a conducting film before straining is given by

$$R_0 = \rho * \frac{L_0}{A_0}, \tag{2}$$

where ρ is the resistivity and A_0 is the initial cross-section of the film. L_0 is the initial distance between the contacts and equals the gauge length. During straining, the sample geometry changes leading to an increase of the distance between the contacts and a decrease in the cross-section of the film. Furthermore, microstructural modifications as necks, cracks, dislocation pile-ups at grain boundaries or buckles occur, depending on the maximum strain and whether a brittle or ductile film is investigated. Necks and cracks form perpendicular to the straining direction. Both effects cause the electrical resistance of the film to increase during straining.

The instantaneous resistance R during straining is given by:

$$R = \rho * \frac{L}{A}, \tag{3}$$

where $L=L_0+\Delta L$ is the instantaneous distance between the contacts and A is the instantaneous cross-section.

Assuming that the film resistance during straining increases only because of elastic deformation of the sample, the relative resistance during straining can be approximated by:

$$\frac{R}{R_0} = \left(\frac{L}{L_0}\right)^2 = (1 + \varepsilon)^2, \quad (4)$$

where $\varepsilon = \Delta L/L_0$ is the applied strain. Hereafter Eq. 4 is called theoretical line for elastic deformation and can be seen in Figure 7 (b) (black dotted line).

At higher strains, when plastic deformation takes place and structural modifications (necking, cracking, buckling, delamination, etc.) occur, the relative resistance deviates from the theoretical line (Eq. (4)) and it is no longer applicable. The resistance is then difficult to describe by an analytical formula. The deviation correlates with the transition from the linear to the non-linear regime of the stress-strain curve (Figure 7).

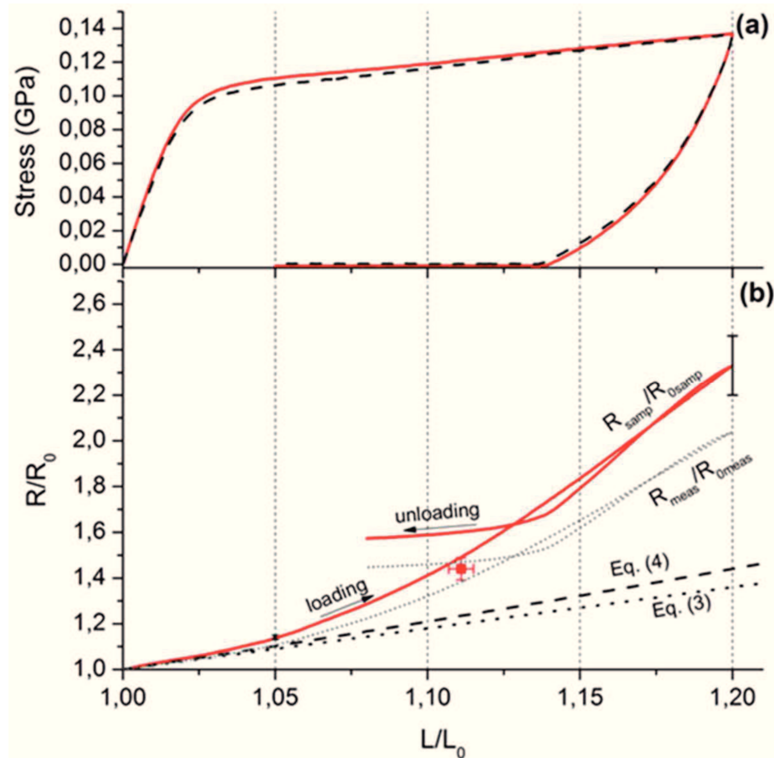

***Figure** 7: Exemplary curves derived in an in-situ 4PP experiment: (a) Engineering stress vs. realtive elongation, (b) Relative resistances R/R_0 vs. relative elongation. R_{meas}/R_{0meas} and R_{samp}/R_{0amp} equal the measured and corrected relative resistance respectively. The solid square shows the corrected relative resistance recorded 24 h after tensile testing and indicates relaxation processes. Eq. (4) represents the theoretical line for elastic deformation. Eq. (3) can be neglected [6].*

The resistance measured during straining R_{meas} consists of two parts: R_{samp} , which is the resistance of the part of the sample being strained and R_{const}, a resistance that remains constant during straining.

$$R_{meas} = R_{samp} + R_{const} \tag{5}$$

R_{const} can be associated with a contact resistance, the resistance of the film under the grips, or the resistance of a conductive paste. In order to interpret the measured data correctly and not to underestimate the resistance growth, R_{const} needs to be carefully estimated and subtracted from the measured values (Figure 7).

During unloading resistance recovery takes place. The resistance decreases due to decreasing contact distances, increasing cross-sectional area and closure of small or bridging of larger cracks. With polymer substrates, further resistance recovery can take place after unloading due to viscoelastic relaxation of the substrate. Both geometrical shrinkage of the sample and closure of present cracks happen during relaxation processes and lead to a decreasing resistance after unloading [24].

2.4 Electrical properties of thin metal films on polymer substrate

The resistivity of a thin metal film is generally higher than the resistivity of bulk material due to increased electron scattering. In bulk materials electron scattering stems mostly from thermal vibrations of the lattice. The resistivity of thin films increases with decreasing film thickness for two main reasons. Due to the deposition process the structure of thin films is normally more disordered, having smaller grains with a higher dislocation and defect density. Therefore, electron scattering occurs increasingly at the grain boundaries. At very small film thicknesses a second effect occurs, namely electrons become scattered from surfaces and interfaces. As a result the resistivity of a physical vapour deposited (PVD) gold film increases from $2.2 * 10^{-8}$ Ωm, the value of bulk material, up to $2.4 * 10^{-8}$ Ωm [25].

Microstructure, such as grain size or the presence of cracks, also influences the electrical properties. Larger grains are preferable for a low resistance, due to fewer grain boundaries where electrons become scattered. The electrical resistance is very sensitive to the presence of cracks. Cracks perpendicular to the current flow form obstacles for the electrons and as a result, increase the resistance of the film. Therefore, measuring the alteration of the resistance of a metal film can serve as a way to determine the presence of cracks.

2.4.1 Electrical testing

To measure the electrical properties of thin gold films on polyimide a custom-made test configuration is used in this work. A detailed description of the principle setup is given in Chapter 3.5. In the following paragraphs the physical principles of electrical testing are explained. The current density J can be calculated by:

$$J = \frac{I}{\delta * w}, \quad (6)$$

where I equals the applied current, δ is the thickness of the metal film and w is the width of the sample. To obtain electromigration an extremely high current density ($J \sim 10^6$ A/cm^2) is required. Occurrence of electromigration alters the resistance of the metal film due to changes in the microstructure.

When current is run through a conductor a part of the electrical energy is transformed into thermal energy. This effect is known as Joule Heating or resistive heating and causes the temperature of the conductor to increase. The amount of the generated heat P is proportional to the square of the applied current I:

$$P = R * I^2. \quad (7)$$

Therefore, even small currents can produce substantial Joule Heating and cause the temperature of the conductor to increase significantly. High currents can cause the polymer substrate to melt [26].

The electrical resistance R of most materials is temperature dependent (Eq. 8):

$$R = R_0 * (1 + \alpha * \Delta T) \quad (8)$$

R_0 is the initial resistance at an initial temperature T_0, α is the thermal coefficient of resistance and $\Delta T = T - T_0$ is the difference between the actual temperature T and T_0. The thermal coefficient of resistance for gold is $\alpha = 0.0034$ /K [27]. Therefore, increasing temperature causes the resistance to rise. Eq. 7 and Eq. 8 can be used to estimate the actual temperature of the sample. By measuring R_0 at a very low current ($I \sim 0.01$ A) and R at a certain testing current the temperature increase can be calculated. This value can serve as an estimation of the sample temperature since heat is drawn away.

Electrical testing is performed over varying time frames and at different current densities to investigate the electrical stability of the films and occurrence of potential electromigration. Compared to in-use conditions this is an accelerated electromigration test. Higher

current densities imply shorter times until electromigration occurs. The obtained data can then be extrapolated to long-term behaviour at in-use conditions (Black Law Chapter 2.5.2).

2.5 Electromigration

Electromigration is a current-driven self-diffusion mechanism of metal atoms. It can occur at sufficiently high current densities in all metallic components of integrated circuits, which carry electric current, and causes the loss of current carrying capability or the occurrence of electrical short circuits [10]. Thin films, used as conductors in microelectronic devices, are especially prone to electromigration effects. Their microstructure provides a large number of rapid low- temperature diffusion paths, such as grain boundaries or interfaces, that allow a significant mass transport [5]. Decreasing interconnect dimensions and increasing current densities during operation demand, that a tremendous amount of effort is put into research on how to impede electromigration and thereby prolong the lifetime of microelectronic devices.

An electric field applied across a conducting line causes an electron flow counter to that field, from the cathode to the anode. At high current densities and sufficiently high speed of electrons a significant momentum transfer takes place from moving electrons to nominally stationary metal ions, forcing the ions to move in the same direction as the electron flow (electron wind force). On the other hand, an electrostatic force due to that applied field tends to move the positively charged metal ions in the direction opposite to the electrons. The electron wind force predominates and the result is a net drift of ions along the conductor in the direction of the electron flow. Grain boundaries, defects, free surfaces and interfaces are primary diffusion paths of the ions. It was shown that the most dominant diffusion path varies for different materials. It depends on the lattice structure, the microstructure of the sample, the presence of dopants and the presence of adhesive surface layers (i.e. native surface oxide in Al) [10, 28, 29, 5].

The material flux results in an accumulation of material at the anode and depletion towards the cathode. The structure of the line changes, as hillocks and voids are formed at the anode and cathode, respectively. Due to the flux, a stress gradient is created along the line with compressive stress induced in accumulated regions and tensile stress in regions of depletion. The stress gradient counteracts the electromigration and drives the diffusive mass

transport in the opposite direction, from compressive towards tensile stress. This so called back stress increases with decreasing line length leading to a critical line length, L_{th} (Blech Length), where the back stress exceeds the wind force. Below L_{th} electromigrative mass transport is completely negated and no change in structure occurs.

The atomic flux, J_a, is mainly the result of those two opposing driving forces mentioned above, the electron wind force and the back stress and can be described by the following equation [28]:

$$J_a = -\frac{DC}{kT} * \left(Z^* eE - \Omega * \frac{\delta\sigma}{\delta x}\right), \tag{9}$$

where D is the diffusion constant, C is the concentration of atoms, k is Boltzmann's constant, T is temperature, Z^* is the effective charge number, e is the fundamental electronic charge, E is the electric field, Ω is the atomic volume, and $\delta\sigma/\delta x$ is the stress gradient along the line.

Eq. 10 shows the influence of temperature on the diffusion constant:

$$D = D_0 * e^{-\frac{E_a}{kT}} \tag{10}$$

D_0 is the maximum diffusion coefficient at infinite temperature and E_a is the activation energy. E_a varies for different diffusion paths. Temperature strongly influences diffusion for it determines the amount and velocity of moving ions. Therefore, increasing temperature strongly promotes electromigration. Every parameter that influences diffusivity, such as microstructure, density of vacancies, melting point of the material etc., has an influence on electromigration as well.

2.5.1 Drift test

Although it is not used in this work, a short explanation of the experimental configuration and the basic principle introduced by Blech in 1976 will be given here, due to the importance of the drift test in electromigration studies. Stripes of metal with relatively low resistance, whose electromigration response is to be investigated, are patterned over the length L on a metal film such as TiN. The length of the individual stripes varies as schematically shown in Figure 8.

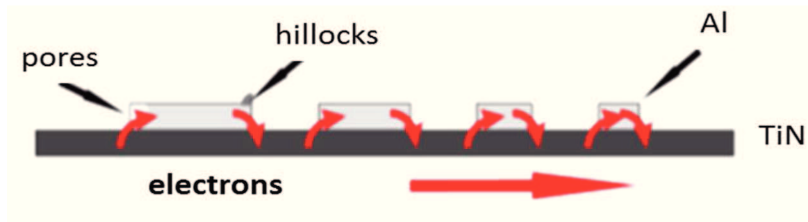

Figure 8: *Schematic setup of the drift test. Metal stripes (Al) of various lengths are patterned onto a conductive Titanium Nitride (TiN) film. The current shunts through the lower-resistance Al stripes [30].*

The metal film has a high melting point and is not susceptible to electromigration under experimental conditions. It is, in turn, deposited on a thick non-conducting substrate. As DC voltage is imposed across the length of the film, the resulting electric current shunts through the lower-resistance stripes over its entire length. At sufficient high current densities electromigration is induced in the metal stripes. As metal atoms drift from the cathode to the anode the entire stripe is displaced over time in the direction of electron motion. Figure 9 shows a schematic of a single stripe under testing condition and the formation of hillocks and voids at the ends [10].

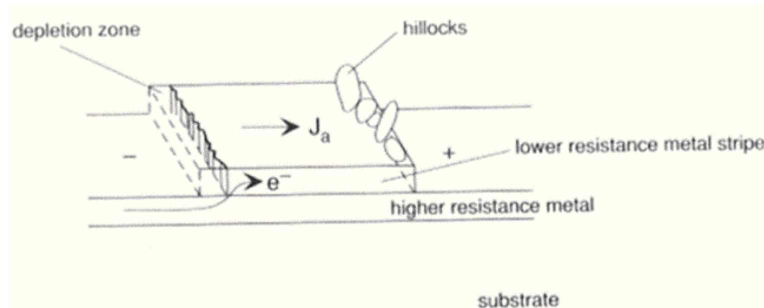

Figure 9: *Single stripe undergoing electromigration. Voids and hillocks evolve at the anode and cathode respectively [10].*

For a given current density, J, there is a critical stripe length L_{th} known as Blech Length to be found, below which no electromigration damage is observed. L_{th} is inversely proportional to the current density. For a given stripe length, there is a threshold current density J_c below which no electromigration occurs. An explanation for this effect was given in Chapter 2.5. J_c also increases with decreasing temperature due to thermal activation.

One can determine the critical product of stripe length and current density $(JL)_c$ below which electromigration does not occur using the following equation:

$$(JL)_c = \frac{\Omega * \Delta\sigma}{\rho Z^* e}, \tag{11}$$

where $\Delta\sigma$ equals the maximum stress within the line and ρ is the resistivity [30]. Furthermore, an electromigration induced drift velocity v_D can be derived by determining the velocity of the negative stripe-end that erodes away [31]. Figure 10 shows the result of a drift test conducted on four aluminium stripes at room temperature with a current density of $J = 3.7*10^5$ Acm^{-2} [10]. The effect of electromigration increases with increasing stripe length whereas the shortest stripe has a subcritical length and shows no damage at all.

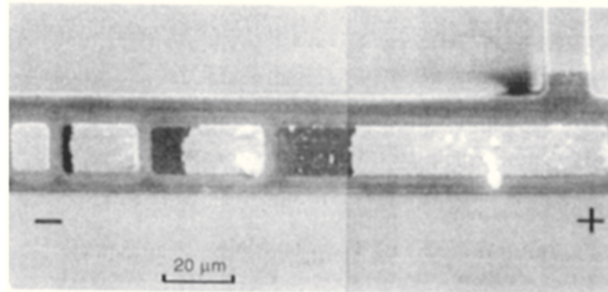

***Figure 10**: Drift test conducted on aluminium ($J=3.7*10^5$ A/cm^2). The effect of electromigration increases with increasing stripe length. The shortest stripe (left) has a subcritical length and shows no damage [10].*

For gold thin films on polyimide substrate it is not possible to manufacture the above discussed Blech structure. Therefore, a different experimental setup is used in this work to investigate the electromigration behaviour of the films.

2.5.2 Electromigration lifetime extrapolation, Black Law

In practice, accelerated electromigration tests are performed at high temperatures and current densities. The obtained data is then extrapolated to long-term in-use conditions, where current densities and temperatures are typically lower, to assess the reliability of microelectronic devices. The extrapolation is commonly based on Black's Law where the median time to failure or 50th percentile fail time of a failure population t_{50} is expresses as [28]:

$$t_{50} = \frac{B}{J^n} * e^{\frac{E_a}{kT}} \tag{12}$$

B is an empirically-determined constant and *n* is the current density exponent. All other symbols have been previously defined. The current density exponent is strongly dependent on temperature and testing conditions and can vary from 1 to above 10. $n > 2$ indicates the presence of Joule Heating. Typical *n*-values are between 1 and 2 dependent on whether void growth or void nucleation is the limiting factor of electromigration respectively [30]. One should note, that t_{50} is a statistical value, meaning that individual lines can fail at essentially shorter or longer times.

3 Experimental

3.1 Starting material

50 nm gold (Au) thin films were sputter-deposited onto a 50 µm flexible polyimide substrate (PI, brand UPLIEX). A 10 nm chromium (Cr) interlayer is used to improve adhesion between the film and the substrate. Figure 11 shows a schematic of the investigated film-substrate systems.

***Figure 11**: Schematics of the investigated film-substrate systems, AuCr: 50 nm Au film sputter deposited onto a 50 µm polyimide substrate. A 10 nm Cr interlayer is used to improve adhesion; Au: 50 nm Au film sputter deposited onto a 50 µm polyimide substrate, no adhesion layer.*

Sputtering was performed with a DC Magnetron system in a similar manner to Yeager et al. [32]. Argon ions were used to sputter the metal atoms. For the gold–chromium samples, 10 nm interlayer of chromium was sputtered onto PI at a pressure of $1.5*10^{-3}$ Torr at 100 W DC power. The chromium-covered samples were then sputtered with gold without breaking vacuum. For gold samples without interlayer gold was deposited directly onto PI. In both cases gold was sputter deposited to a thickness of 50 nm. Typical deposition parameters for the gold layer were a pressure of $7.5*10^{-3}$ Torr and a power of 75 W DC.

Gold is a ductile material whereas Cr shows a brittle behaviour. Due to its low resistivity the gold layer is the charge carrying part of the composite. The Cr interlayer is applied to enhance adhesion between the film and the substrate. The basic functions of the polyimide substrate are to support the metal film and give the required flexibility.

Table 1 gives an overview over relevant material characteristics of the different layers.

Material	Melting point T_m (°C)	Bulk resistivity ρ_B at 20 °C (10^{-8} Ωm) [33]	Lattice	Temperature coefficient α at 20 °C (1/°C)	Function
Au	1064	2.24	fcc	0.003715 [34]	Charge carrier
Cr	1907	13	bcc	~ 0.0004 (Ni-Cr alloy) [33]	Adhesion improve-ment
PI	~ 400	insulator	-	-	Support, flexibility

Table 1*: Overview of relevant material characteristics and functions of the different layers of the film-substrate system.*

3.2 Material characterisation

The film thickness of the gold layer was measured with AFM (Veeco Dimension 3100) in tapping mode. It is approximately 50 nm. The particular thickness of the Cr-interlayer was not determined. It is assumed to have the nominal thickness of 10 nm. The grain size of the gold layer was determined with linear intercept method by using transmission electron microscope (TEM, Philips CM-12) images. The gold film has a nanocrystalline microstructure with a grain size between 20 and 50 nm. The microstructure of the film systems in the initial condition and after different testing methods was characterised using light-microscopy, AFM (Veeco Dimension 3100) in tapping mode and SEM (LEO 1525) using secondary electrons (SE) and backscattered electrons (BSE). AFM imaging was performed with 512 dpi and a scanning rate of 1 Hz to obtain the highest possible resolution. A scan size of 25 µm x 25 µm was appropriate for the obtained crack spacing. The tips used were Nanosensors™ PointProbe® Plus – NCHR with a guaranteed radius < 10 nm and possibly < 7 nm. In order to get accurate height data the height scale of the AFM was calibrated prior to the measurements. Typical settings for SEM imaging were a voltage of 5 kV and a 20 mm aperture. A magnification of 12000x was chosen in order to get a good comparison between AFM and SEM images. For determination of the chemical composition of surface features that evolved during electrical testing, energy dispersive X-ray analyses (EDX) were also performed at the SEM LEO 1525.

3.3 Fragmentation testing

The uniaxial tensile test was performed with an Anton Paar TS 600 straining stage and the corresponding tensile stage control software. A sample (sized ~ 7 mm x 30 mm) was clamped between two straining grips with a minimum distance of 24 mm. Prior to straining any slack in the sample was taken up by carefully manually increasing the displacement until the sample was tight but not strained. This new distance is the initial gauge length. Samples were strained to various maximum strains with a constant displacement rate of 5 µm/s. The crack spacing, λ, (distance between the cracks) of each strained sample was measured using AFM and SEM. AFM images were analysed with GWYDDION [35]. Three surface profiles perpendicular to straining direction were extracted across each image at approximately the same positions. By analysing the surface profiles the number cracks and the distance between them was measured. SEM images were analysed with the software ImageJ [36]. Again lines perpendicular to straining direction were laid across each image at the same positions and the distance between visible cracks was measured.

3.4 Electro-mechanical testing – In-situ 4 Point Probe measurement

The basic concept and theory of electromechanical testing has been explained in chapter 2.3.1. The uniaxial tensile test was performed with an MTS Tyron 250® Universal testing machine. A 4 point probe resistance measurement (Keithley 2000 multimeter) is incorporated into the grips to record the resistance during loading and unloading. Four samples (~ 7 mm x 35 mm) of each film system (Au and AuCr) were strained to a maximum strain of ε = 15 % and unstrained with a constant displacement rate of 5 µm/s. The minimum distance between the grips was constant for each sample at L_0 = 20 mm (gauge length). Before actual straining the initial resistance, R_0, should remain constant for at least 10 to 15 min. Figure 12 (a) shows a schematic of the experimental setup and an image of a mounted sample.

To determine the resistance of the film under the grips, R_{const}, which remains constant during straining, the initial resistance of the film, R_0, was measured with a second four point probe setup prior to electromechanical testing, shown in Figure 12 (b). The distance between the inner contact needles equals half of the gauge length of the tensile test. In order to refer to the same area the measured resistance was multiplied by 2.

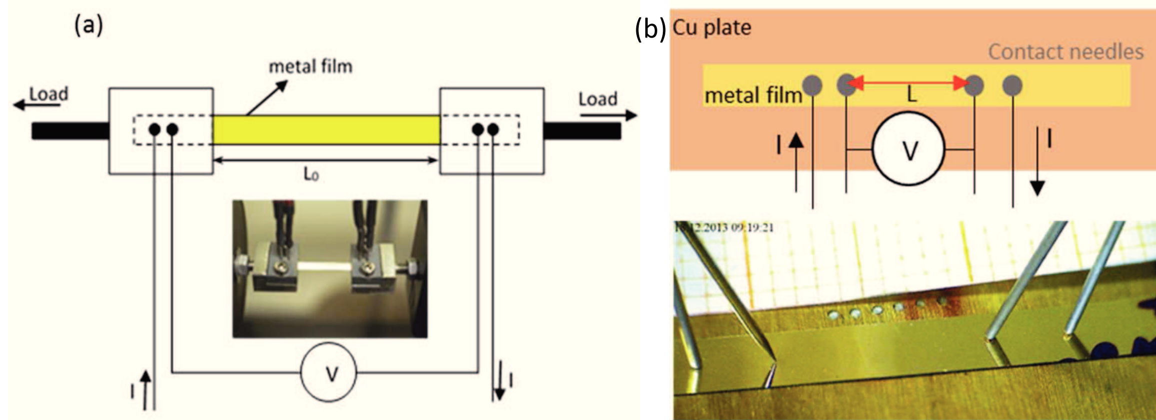

Figure 12: (a) Experimental setup of in-situ 4PP experiment and image of mounted sample [6]. The resistance of a thin film is recorded during uniaxial loading and unloading of the sample. (b) 4 point probe setup for reference measurement of R_0 to determine R_{const}.

3.5 Electrical testing

To determine the electrical properties of a film/substrate couple a custom-made test configuration is used in this work. Two contact needles are attached to the sample surface and force a constant direct current through the film, while the resulting voltage, V, is sensed. The film resistance is calculated using Ohm's Law, $R=V/I$, and recorded over time. In order to always measure an area of equal size the distance between the contact needles is constant for all samples at approximately $L \sim 3$ mm. The complete setup is placed on a copper plate to draw away heat. A thermal paste (Electrolube, HTCP) is placed under the tested region of the sample to increase the thermal stability and prevent burning of the polymer substrate. A camera is installed to provide a magnified image of the sample during testing. Figure 13 shows a schematic of the experimental setup. Two different sample geometries are used to perform electrical testing. The stripe geometry provides an almost constant current density over the cross section of the film. For the cut geometry two artificial cuts are made on both sides of the sample to narrow the area of interest and increase the current density. Both geometries can be seen in Figure 14.

Strained (ε = 15 %) and unstrained samples of Au and AuCr were subjected to various current densities over different time frames while the resistance was recorded over time. After fixing the sample the current density was increased stepwise until a defined current density was reached and held at a constant level. The experiments were stopped after a maximum of 7 days if no significant change in the resistance was observed. Before imaging of

the tested samples with SEM the conductive paste was removed with ultrasonic cleaning treatment.

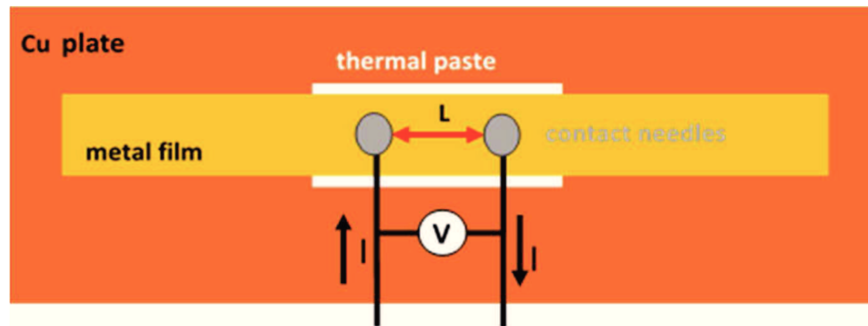

Figure 13*: Experimental setup for electrical testing. A constant current is forced through the film while the resulting voltage is sensed. The film resistance is calculated using Ohm's law and recorded over time.*

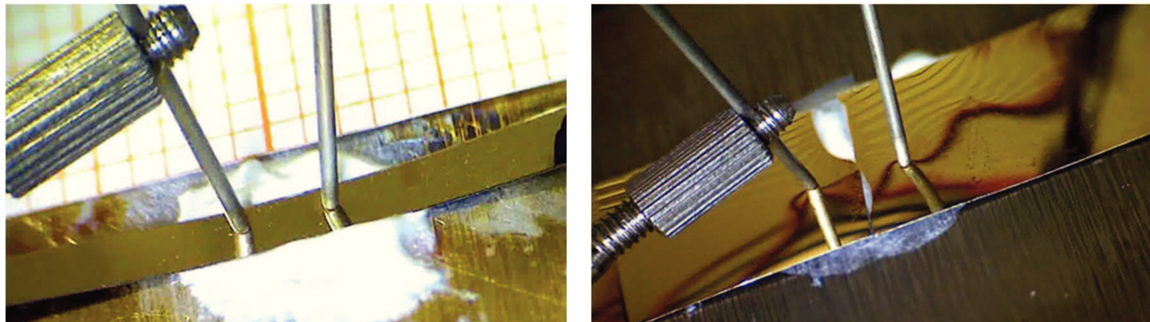

Figure 14*: Different sample geometries used for electrical testing: (a) stripe geometry: constant current density over the cross section; (b) cut geometry: artificial cuts on both sides locally increase the current density and narrow the area of interest.*

4 Results and Discussion

4.1 Fragmentation test

In a pre-trial, Au films with and without Cr interlayer have been strained to maximum strain of ε = 15 % with a uniaxial tensile test. The formation of TTCs perpendicular to the straining direction is observed only in Au films with Cr interlayer. In the ductile Au films without interlayer no cracking occurred. Therefore, fragmentation testing was performed only on Au films with Cr interlayer. Samples of AuCr were strained to different maximum strains equal to ε = 2, 5, 10, 12 and 15 %, respectively. After straining the sample surfaces were imaged with AFM and SEM. The time between straining and imaging was long enough that potential relaxation processes of the polymer substrate were fully developed [6].

An example of the crack spacing measurement with AFM is shown in Figure 15. By comparison of the extracted height profile and the original AFM image TTCs are identified (black arrows). The x-Distance between the cracks is equivalent to the crack spacing, λ. Average values of the crack spacing as well as the standard deviation are calculated for each sample.

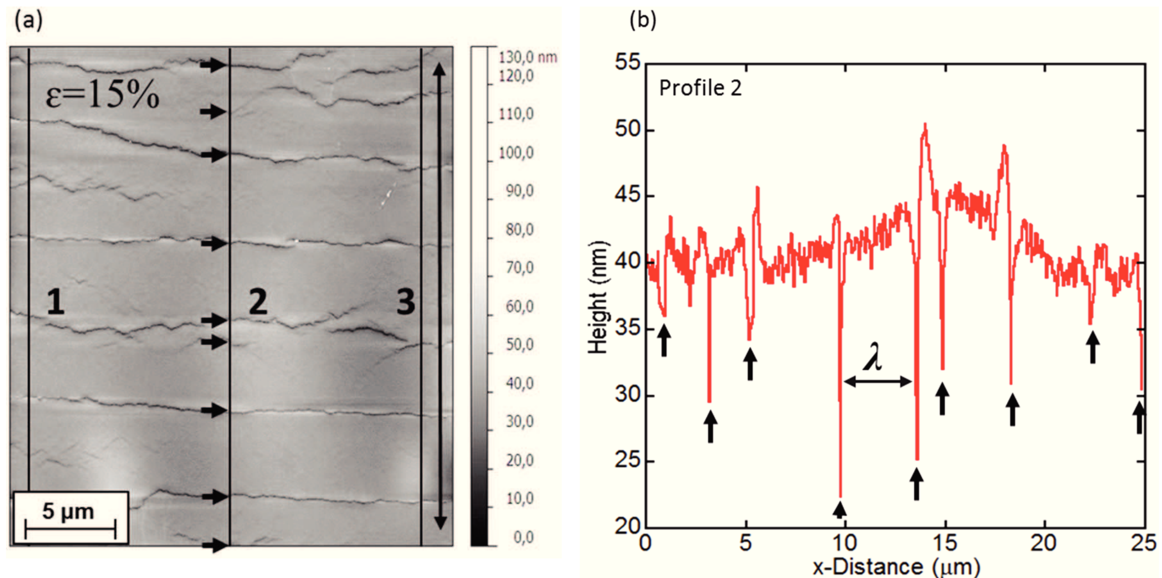

***Figure 15**: (a) AFM height image at 15 % strain of AuCr film. The positions of the extracted surface profiles and the straining direction are indicated. (b) Surface profile from (a) indicating where TTCs have formed (Black arrows). The distance λ is the measured crack spacing between two TTCs.*

Figure 16 shows an example of the crack spacing measurement with SEM. TTCs are identified only by analysing the SEM image along lines laid across (black arrows). Since SEM is not a quantitative surface imaging technique, it is assumed that each crack viewed in the SEM micrographs is a TTC. The distances between the cracks equal the crack spacing and are measured along each line. Again an average value of the crack spacing, λ, and the standard deviation are calculated for each sample.

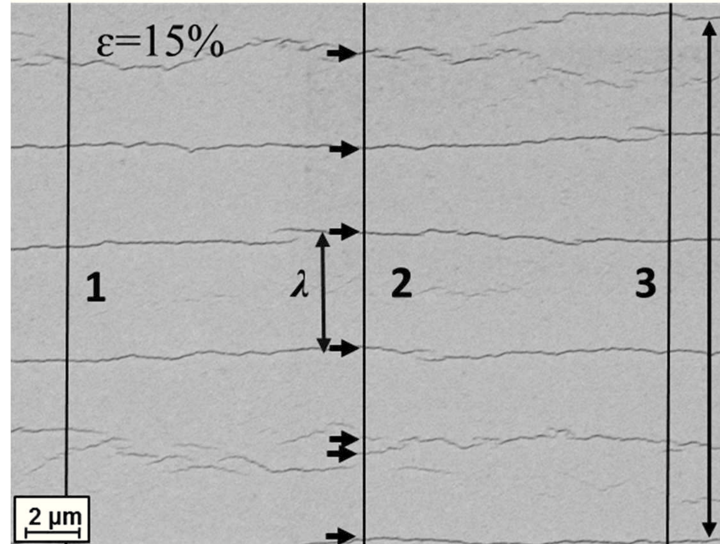

Figure 16*: SEM micrograph at 15% strain of AuCr. Black arrows indicate TTCs. The distance λ equals the measured crack spacing between two TTCs. The straining direction is indicated on the right side of the image.*

Figure 17 shows the crack spacing evolution of AuCr as a function of applied strain for AFM and SEM analysis. Because of the brittle behaviour the two analyses follow one another closely. Cracks are easy to distinguish both in the AFM and SEM. The standard deviation, depicted with error bars, increases with decreasing strain due to the fact that fewer cracks occur.

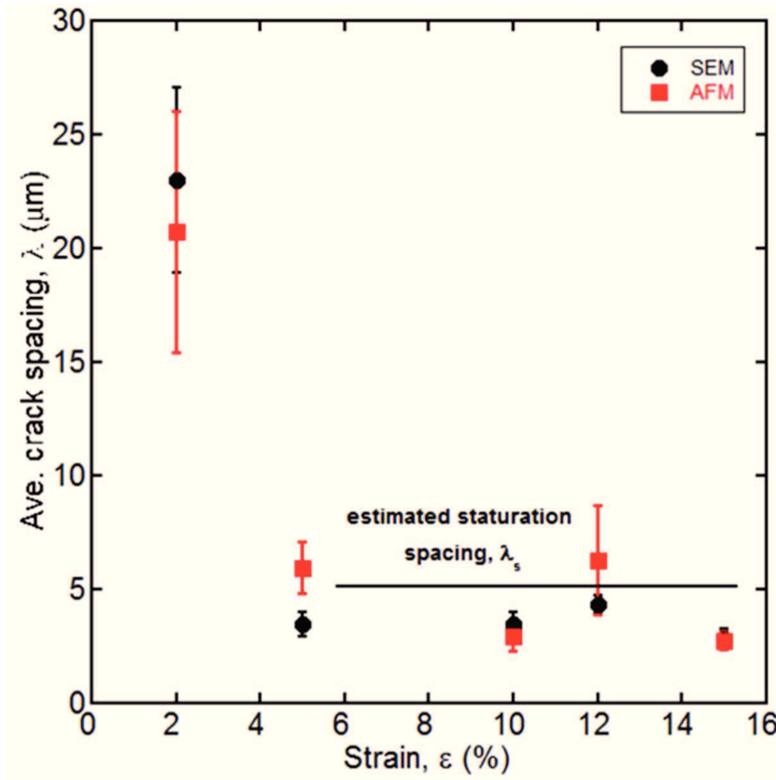

***Figure 17**: Average crack spacing evolution of AuCr as a function of strain. The crack spacing is measured with AFM and SEM. The standard deviation is depicted with error bars. The results follow one another closely. The plateau indicates saturation. Saturation spacing can be estimated with $\lambda_s \sim 5$ µm.*

The 50 nm Au film with Cr interlayer shows brittle behaviour, forming long TTCs at low strains. Saturation occurs at very low strains (saturation strain $\varepsilon_s \sim 4$ %). The saturation crack spacing can be estimated with $\lambda_s \sim 5$ µm. After saturation the cracks open due to stretching of the polymer matrix. Interestingly, buckling delamination between the crack fragments was not observed. The absence of buckling could indicate very good adhesion.

4.2 In-situ 4PP experiment

The initial resistance R_0 of the unstrained samples was measured twice. Once with the in-situ 4PP setup right before straining and prior to that with a second 4PP setup (see Chapter 3.4, reference measurement). The value measured with the in-situ setup is higher due to the contact resistance of the sample under the straining grips. By comparison of those two values the contact resistance under the grips R_{const} was identified. The contact resistance is approximately 0.5 Ω for both film systems and is subtracted from the total resistance measured during the in-situ experiment in order to not underestimate the resistance increase.

Figure 18 shows a comparison of the electro-mechanical behaviour of Au and AuCr strained to a maximum strain of ε = 15 %. The plotted curves show the calculated average of the four tested samples for each film system. For better distinguishability the standard deviation is only shown for representative points in form of error bars.

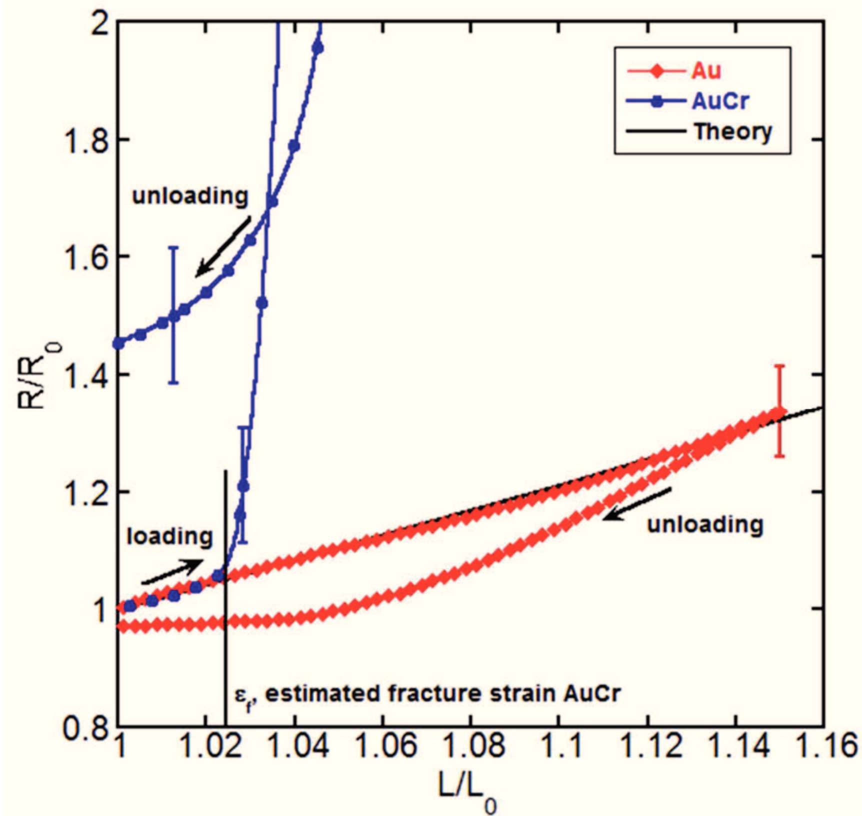

***Figure 18**: Change of the normalized electrical resistance R/R_0 with increasing normalized length L/L_0 during straining of Au and AuCr, ε_{max}=15 %. The curves show the calculated average of four tested samples for each system. Error bars depict the standard deviation at representative points. The obtained behaviours strongly differ from each other.*

Table 2 complements Figure 18 and summarises characteristic data obtained in the in-situ 4 point probe experiment for both film systems.

Material	R_{const} (Ω)	R_0 (Ω)	$R/R_{0\ max}$	$R/R_{0\ End}$
Au	0.5	3.5	1.34	0.97
AuCr	0.5	3.67	8.30	1.46

***Table 2**: Summary of characteristic data of Au and AuCr from Figure 18.*

The observed performances strongly differ from each other. Au films with Cr interlayer show a brittle behaviour. The curve deviates from the theoretical line for elastic deformation during straining due to the formation of TTCs perpendicular to straining direction. The fracture stain can be estimated to be about ε_f=2 %. After reaching the fracture strain the resistance increases rapidly during loading. The number of cracks increases until saturation is reached. Then cracks open due to stretching of the polymer substrate. Despite crack evolution no complete electrical failure is observed at a maximum strain of 15 % (not shown in Figure 18). The maximum normalised resistance at 15 % strain $R/R_{0\,max}$ is 8.3, more than 8 times higher than the initial normalised resistance (Table 2). Individual cracks propagate through the thickness of the metal layer but not over the whole width, leaving bridges for electrons to flow (Figure 19 (a)). During unloading the resistance decreases with the same slope as evolved cracks close and more and more crack-edges overlap and get in contact again. The final resistance R_{end} is about 50 % higher than the initial resistance R_0 though, indicating the presence of cracks. Preservation of electrical conductivity on the other hand provides evidence of the presence of crack bridges. Both TTCs and crack bridges can be seen in an AFM image taken after testing (Figure 19 (a)). At the time of imaging eventual relaxation processes of the polymer substrate were fully developed [6].

As expected, the 50 nm Au films without Cr interlayer illustrate very ductile behaviour. Furthermore, they show outstanding electromechanical properties. The resistance follows very closely the theoretical line, with R/R_0 increasing only because of elastic deformation during straining. There is no evidence of severe plastic deformation in the form of localized necking or fracture. The maximum normalised resistance at 15 % strain $R/R_{0\,max}$ is 1.34. During unloading the curve comes below the theoretical line. Underestimation of the constant resistance R_{const} could be one explanation for that. The final resistance R_{End} is approximately the same as the initial resistance. Figure 19 (b) shows the surface of Au after testing. No cracks perpendicular to the straining direction can be seen nor localized thinning (necking) to indicate plastic deformation.

The features parallel to straining direction in Figure 19 (b) stem from the deposition process. Their shape changes during straining as they are elongated in straining direction. Interestingly the features do not initiate cracking perpendicular to straining direction, which indicates very ductile behaviour of the 50 nm Au films.

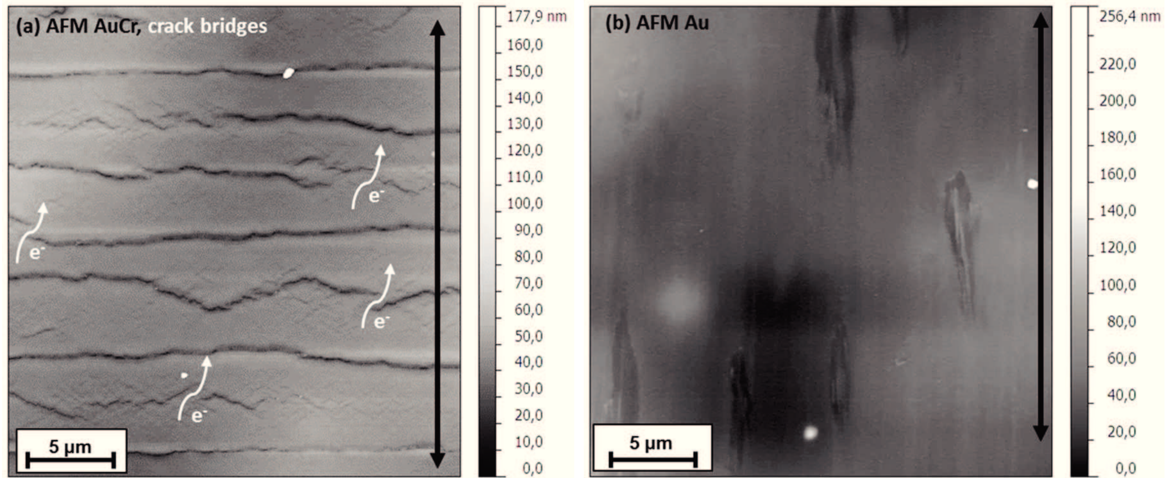

Figure 19*: AFM images of the sample surface after electromechanical testing, ε = 15 %,straining direction is indicated, (a) AuCr: TTCs perpendicular to straining direction can be seen; (b) Au: no evidence for localized thinning (necking) or TTCs perpendicular to straining direction. The features parallel to straining direction stem from deposition and elongate during straining.*

4.3 Electrical testing

The influence of high current densities on thin gold films on polyimide is investigated in this work. As deposited Au and AuCr samples are subjected to various current densities over different time frames while the resistance is recorded. Since the influence of high current densities on micro-cracks is of special interest AuCr samples strained to ε = 15 % are tested with the cracks perpendicular to the direction of the applied current. For the calculation of the current density, *J* (Eq. 6), the nominal film thickness δ = 50 nm of the gold layer is used for both film systems. The 10 nm Cr layer is neglected for the AuCr system due to its high resistivity.

$$J = \frac{I}{w * \delta} \tag{6}$$

For the stripe geometry *w* equals the mean width of the sample between the contacts. For the cut geometry the distance between the cuts equals *w* in Eq. 6.

Figure 20 shows a map of the performed electrical treatments. Some general statements can be derived from this map. In a pre-trial the experimental setup was tested. By successive improvement of the testing conditions (Cu plate = heat sink, thermal paste), the applied current densities and time frames can be increased compared to the pre-trial. The obtained behaviour can be generally divided into two categories. Above a critical limit of the current density ($J \sim 1.5$ MA/cm²) all samples fail after a certain time. Below that limit

the samples either fail or survive the electrical treatment. The value of interest during this test is the alteration of the recorded resistance at a constant testing current density. An experiment is stopped after a maximum of 7 days if no significant change in the recorded resistance is observed.

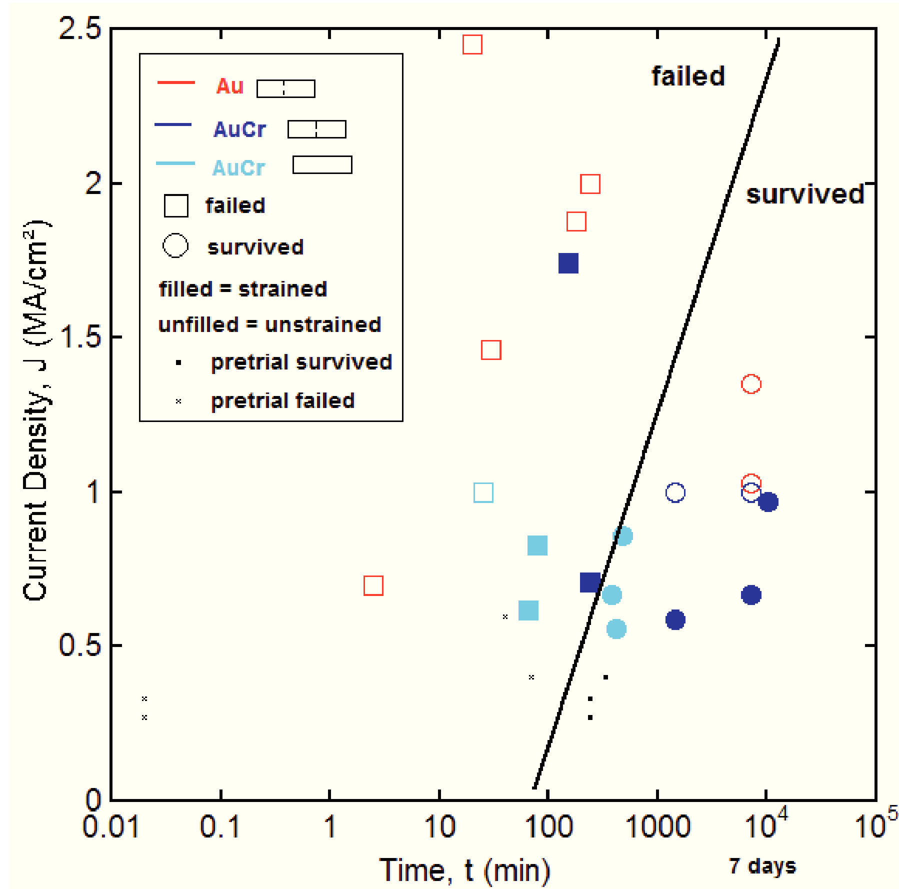

Figure 20: *Map of electrical treatments, Au and AuCr samples are exposed to different current densities over various time frames. Above 1.5 MA/cm² all samples fail, below that value the samples ether survive the treatment or fail after a certain time. For surviving samples experiments are stopped after a maximum of 7 days if no significant change in the recorded resistance is obtained.*

Failure occurs in the form of local decomposition of the polymer substrate ($T_s \sim 400$ °C). In the stripe geometry failure occurs at the contact needles whereas the cut geometry fails in-between the cuts in the reduced area. The temperature increase due to Joule Heating is estimated using the recorded resistance data (formula given in Chapter 2.4.1) and should not exceed $\Delta T = 150$ °C. The experiments are conducted at room temperature and therefore the absolute sample temperature is below the melting point of the polyimide. Local inhomogeneities however can lead to locally higher current densities and temperatures.

Figure 21 and 22 show exemplary SEM images of failed and survived Au and AuCr samples after electrical testing. The tested regions between two artificial cuts can be seen. Their appearances vary for several reasons and will be explained in more detail below. Not all of the obtained phenomena can be explained yet.

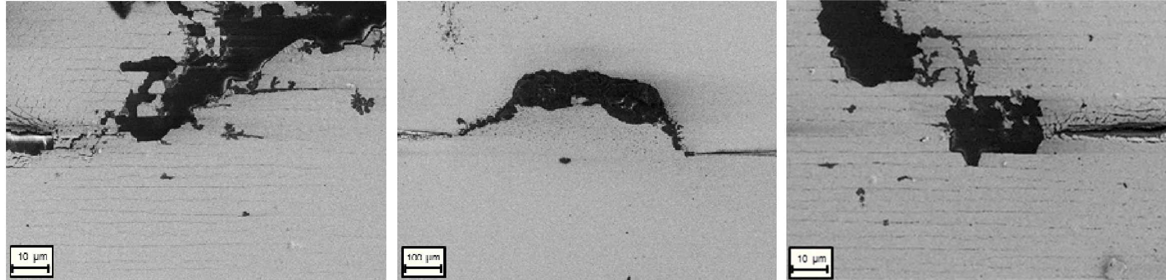

(a) *AuCr, ε = 15 %, J = 0.71 MA/cm², t = 4 h, failed, left and right images are magnifications of the cut tips.*

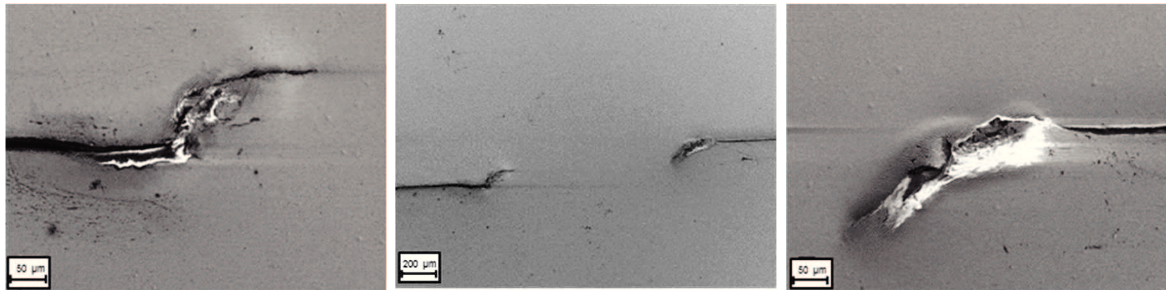

(b) *AuCr, ε = 0 %, J = 1 MA/cm², t = 5 days, survived, Defects at the cut tips are introduced during cutting, left and right images are magnifications of the cut tips.*

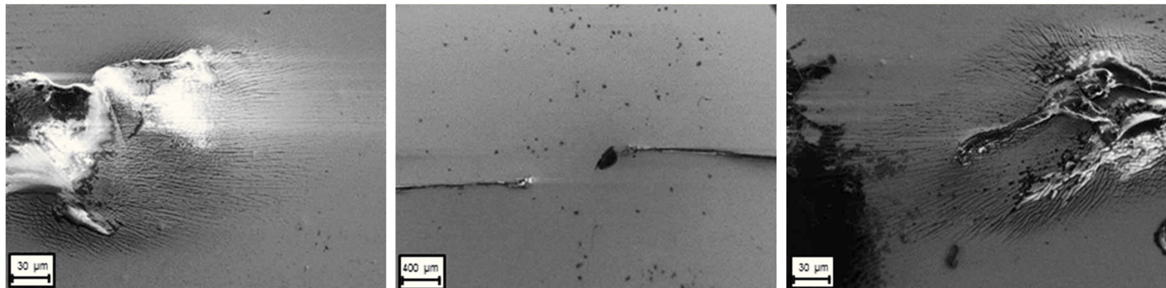

(c) *AuCr, ε = 0 %, J = 1 MA/cm², t = 24 h, survived, cracks parallel to cutting direction form at the cut tips during cutting in brittle AuCr, left and right images are magnifications of the cut tips.*

Figure 21*: Failed and survived samples of AuCr, strained and unstrained. Failure occurs in form of local decomposition of the polymer substrate. Microstructural changes occur preferentially at the cut tips. Long term failure can be explained by electromigrative change of the microstructure (see Chapter 4.3.1.3).*

Figure 21 above shows strained and unstrained AuCr samples after electrical testing. The middle images show an overview of the tested regions between two artificial cuts. The

left and right images are magnifications of the cut tips for better recognisability of the microstructure.

In Figure 21 (a) a strained sample (ε = 15 %) that failed between the cuts after 4 hours at an applied average current density of J = 0.71 MA/cm² is provided. The large black spots indicate a local decomposition of the polymer substrate. The decomposed area is located between the cut tips and is spread out towards the direction of the current. Its shape depends, amongst other factors, on the position of the cuts relatively to each other. Long term failure can be explained by an electromigrative change of the microstructure (evolution of holes), leading to locally higher current densities. Such holes can be seen in the middle image as small dark spots below the decomposed area. Unfortunately no revealing optical analysis of the failed surface is possible once the polymer substrate decomposes. At higher magnifications (left and right image) one can see TTCs perpendicular to the direction of the current. The cracks generated during straining promote failure at lower current densities or shorter times.

In Figure 21 (b) an unstrained AuCr sample that survived the electrical treatment of J = 1 MA/cm² for 5 days is shown. No local decomposition or microstructural changes can be seen in the middle overview image. Magnifications of the cut tips (left and right image) reveal defects at the cut tips that are introduced during cutting. Cutting must be performed carefully in order to avoid these types of defects. They can lead to locally inhomogeneous current densities. In the present case these defects did not lead to future failure of the samples. They can, however, influence the sample lifetime at higher testing current densities.

Figure 21 (c) shows an unstrained AuCr sample after 24 hours of electrical treatment with a current density of J = 1 MA/cm². The sample survived the electrical treatment. The large black spot between the cuts (middle image) could be either early stage local decomposition of the polymer substrate or a contaminant remnant of the conductive paste. Since the smaller dark spots are spread across the whole image and also present in untested regions they are more likely contaminates. Higher magnifications of the cut tips (left and right image) reveal a drawback of the cut-geometry for AuCr samples. One can see cracks at the cut tips parallel to cutting direction that are generated in the brittle AuCr during cutting. These cracks further emphasize the brittle behaviour of AuCr and need to be taken into account as they change the starting conditions for electrical testing.

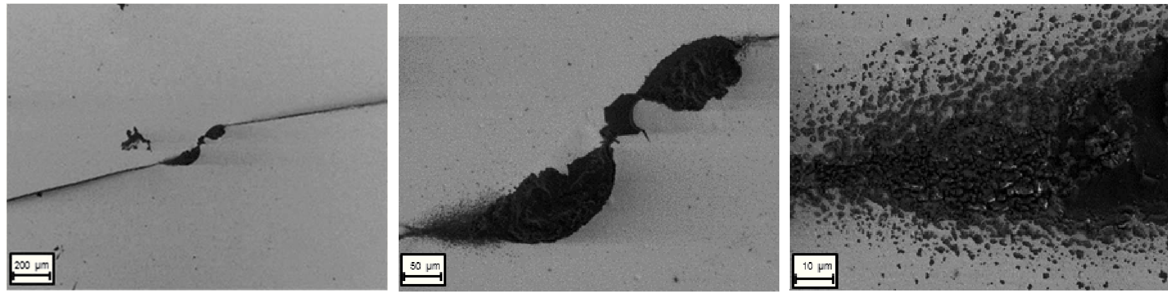

(a) *Au, J = 2 MA/cm², t = 4 h, failed, various magnifications*

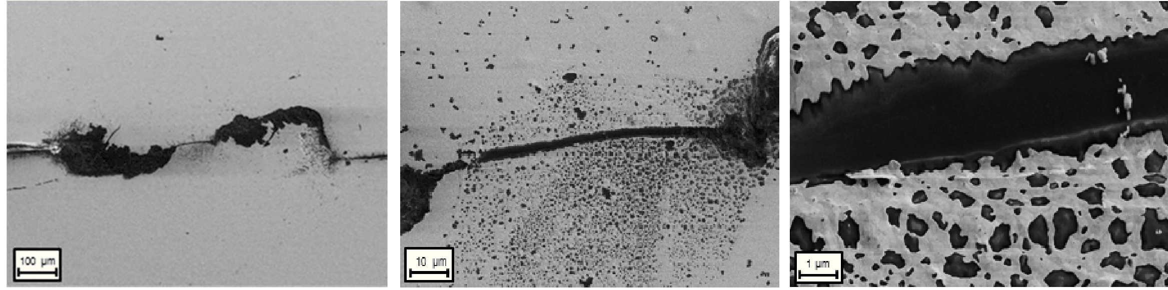

(b) *Au, J = 1.88 MA/cm², t = 3 h, failed, various magnifications*

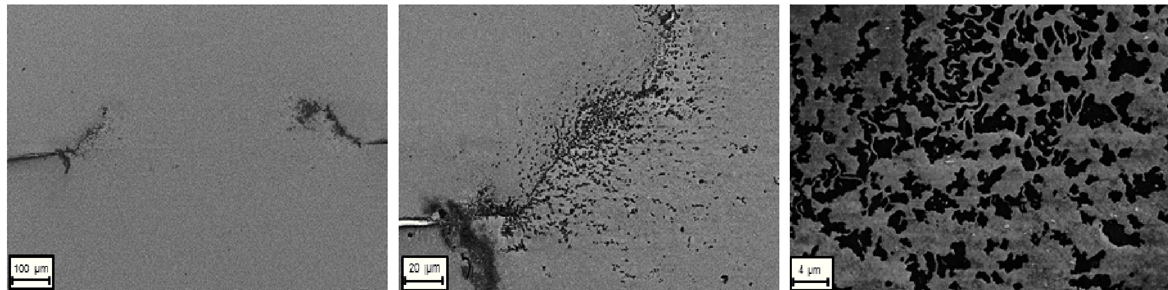

(c) *Au, J = 1.03 MA/cm², t = 5 days, survived, microstructural changes at the cut tip, various magnifications*

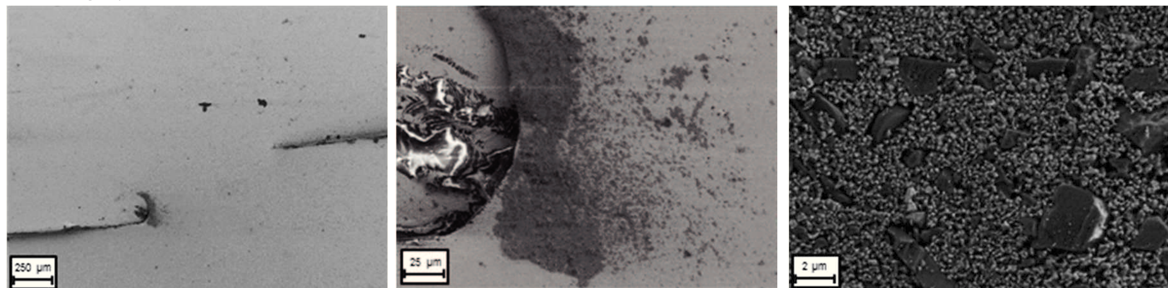

(d) *Au, J = 1.35 MA/cm², t = 5 days, survived, microstructural changes at the cut tip, various magnifications*

Figure 22*: Failed and survived samples, Au, all unstrained. Failure occurs in form of local decomposition of the polymer substrate. Microstructural changes occur preferentially at the cut tips. Long term failure can be explained by electromigrative change of the microstructure (see Chapter 4.3.1.3).*

Figure 22 shows unstrained Au samples after electrical testing. The left images show an overview of the tested regions between two artificial cuts. From left to right the micrographs show higher magnifications of interesting areas for better recognisability.

Figure 22 (a) and (b) show tested Au samples that failed after 3 and 4 hours, respectively, at a current density of ~ 2 MA/cm². Again, large dark spots indicate a local decomposition of the polymer substrate. The appearance of the decomposed regions is different, due to many different influencing factors that are yet to be fully understood. Both areas are s-shaped. It is believed that smaller dark spots in Figure 22 (b) above and below the failed area are holes evolved during testing due to electromigration. If one takes a closer look at the edges of the decomposed area (Figure 22 (b), right image), the impression is created that holes consolidate leading to failure of the sample. Unfortunately no revealing optical analysis of the failed surface is possible once the polymer substrate decomposes.

In Figure 22 (c) and (d), Au samples that survived the electrical treatment of ~ 1 MA/cm² for 5 days are shown. Microstructural changes occur preferentially at the cut tips. The small flower-like dark spots in Figure 22 (c) are believed to be holes that evolve during electrical testing and give evidence of electromigration. The very porous surface structure in Figure 22 (d) could be either hillocks forming during electrical testing due to electromigration or remnant contaminates from the thermal paste. However, the sample is cleaned with ultrasonic treatment prior to imaging and it is unlikely that remnant contaminates remain on the surface. It has been mentioned before that not all of the obtained phenomena can be explained yet.

Returning to Figure 20, the map of electrical treatments, one explanation for failure and the scattering of the results at lower current densities is that defects are created by exceeding the limit current density for rapid failure during initialisation. At the beginning of each experiment the current density, J, is increased stepwise up to a defined testing current density. The testing current density is determined in pre-experiments. The value is chosen that way that no immediate failure of the sample occurs and long term behaviour can be investigated (upper limit). On the other hand, it has to be high enough to obtain a change in resistance and potential electromigration effects at reasonable times (lower limit). A com-

promise between those two criteria has to be found. Since the influence of high current densities is to be investigated in this work, the chosen testing current densities are closer to the upper limit.

Since the experimental setup is very sensitive (amount of thermal paste, film thickness, sample width, distance of contact needles, etc.), the pre-determined upper limit value of the current density (immediate failure) varies and can be easily exceeded. Observation of the recorded resistance during initialisation reveals whether the testing current density is chosen correctly. A very rapid ongoing rise of the resistance indicates instant failure. If the obtained resistance increase at the pre-defined testing current density is too steep, the current density is decreased and the experiment is carried out at a lower current density. In this way defects could have been created leading locally higher current densities and future failure of the sample. Figure 23 shows an exemplary R/R_0 graph of the initialisation phase where the critical value of J for instant failure is exceeded (red mark) and the test is performed at a lower testing current density.

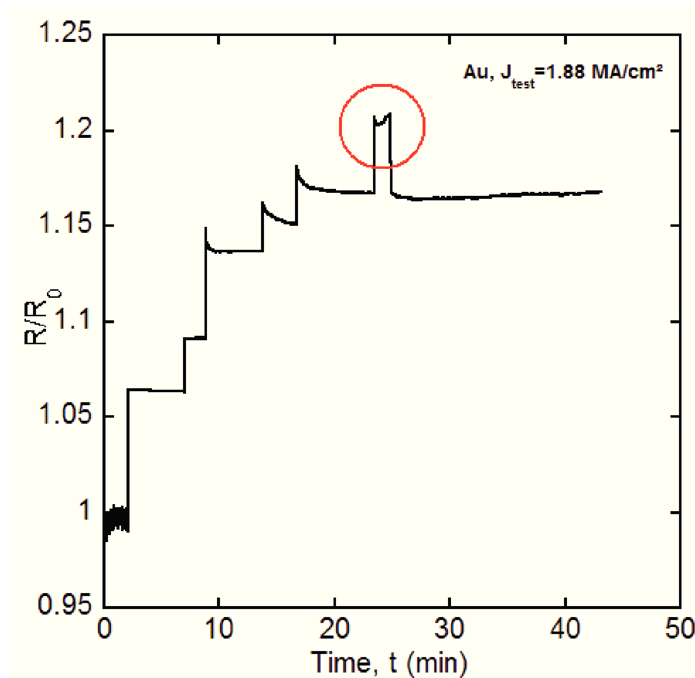

Figure 23: *Initialisation phase of the electrical testing, the red circle marks the region were the critical limit of the current density is exceeded (rapid increase of* R/R_0*), subsequently the current density was decreased and the testing was performed at a lower value.*

Figure 20 also shows, that the cut geometry allows for higher applied current densities and longer times compared to the stripe geometry. This can be explained by the limited area with high current density between the cuts. A large area around the cuts is available to dissipate heat and prevent thermal failure. Furthermore, imaging after testing is facilitated since the area of interest is smaller. Cuts have to be implemented carefully in order not to create defects at cut tip. During testing the thermal paste softens, penetrates through the cuts and propagates over the sample surface due to a temperature increase. Penetration of the paste in the cuts ensures electrical isolation of the two sides and the current density between the cuts is calculated accurately. Propagation of the paste during testing can alter the recorded resistance. A drawback of the cut-geometry is cracks that evolve during cutting only in the brittle AuCr parallel to cutting direction (Figure 21 (c)).

From the map of electrical treatments one can see that higher testing current densities can be achieved in Au films without Cr interlayer than in those with Cr interlayer. Furthermore unstrained AuCr samples can endure higher current densities than strained ones. TTCs perpendicular to the direction of electric current increase the probability of failure.

Figure 24 shows exemplary curves of the normalised resistance recorded during testing as a function of time for strained and unstrained Au and AuCr (all cut-geometry) at a current density of $J \sim 1$ MA/cm². At the beginning of each experiment the initial resistance of the sample R_0 is measured with a low current of $I = 0.001$ A to exclude thermal effects. By normalising the resistance influences like varying sample width or thermal paste can be eliminated. The difference in the R/R_0 values has several reasons. Au and AuCr have a different thermal coefficient of resistance. Different microstructure in AuCr (strained/unstrained) leads to different R/R_0 values of strained and unstrained samples. Due to slightly changing sample geometry different currents are used to obtain the same current density. The temperature increase is proportional to the square of the applied current (Joule Heating, Chapter 2.4.1). The increase in resistance is proportional to the temperature increase (temperature dependence of R, Chapter 2.4.1). Consequently, the resistance increase is higher with higher applied currents leading to different R/R_0 values at the same current densities.

The curve shapes do not differ significantly from each other. All samples survived. No strong alteration of the resistance is obtained during testing. Therefore, the experiments were stopped after 5 or 7 days. The deviations at the beginning stem from initialisation and

manual adjustments and can be neglected. This extends to the sharp increases in the orange and blue curve at 4 and 6 days respectively. In those two cases the testing current density is slightly increased during testing to increase the probability of electromigration.

The testing method is very sensitive. Small variations of the resistance in Figure 24 can be evidence of electromigration due to changes in microstructure of the film but also changes in the testing conditions. Changing testing conditions during the experiment can be a change in room temperature (i.e. from opening a window) or propagation of the thermal paste due to softening.

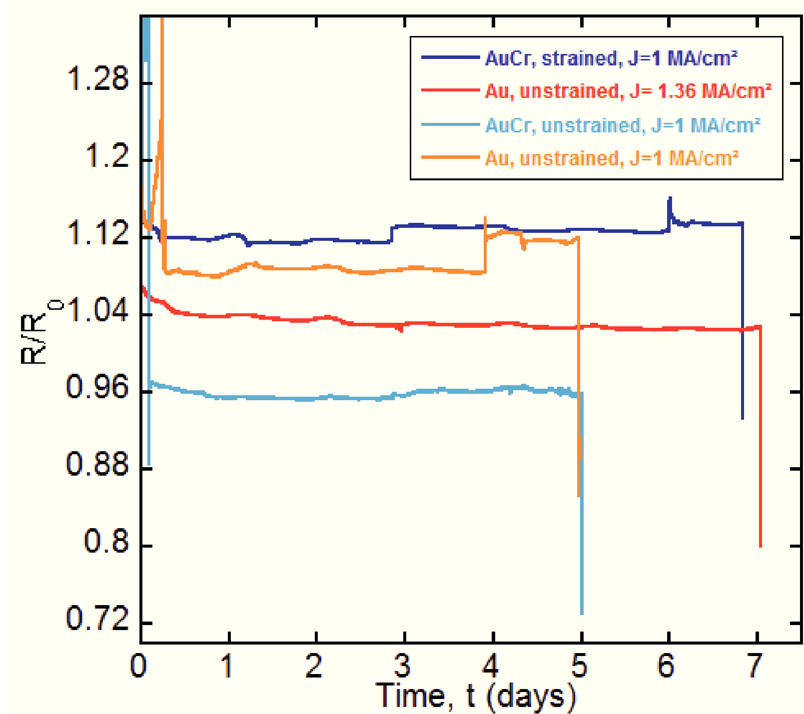

***Figure 24**: Normalised resistance over time for Au and AuCr, strained and unstrained, all cut-geometry. The curves do not differ significantly from each other. The experiments were stopped after 5 and 7 days. Variation of the recorded resistance can be evidence of electromigration or changing testing conditions. The jumps in the orange and blue curve stem for manual manipulation and can be neglected.*

At the end of the experiment the resistance of the sample is again measured at a very low current of $I = 0.001$ A. Compared to the initial resistance R_0 this final resistance R_{End} is generally lower (Figure 24). This gives evidence of a change in the microstructure or point defect density. Grain growth due to thermal treatment during testing could explain the decrease in resistance.

4.3.1 Electromigration

Literature [4, 5] suggests that electromigration generally occurs at current densities $J \geq 1$ MA/cm². In ultra-thin Au films electromigration effects were obtained at much lower current densities of $J = 10^5$ A/m² (= 10 A/cm²) at elevated temperatures [37]. Due to the low melting point of the polyimide high current densities are hard to reach in metal films on flexible polymer substrates. During electrical testing two phenomena which indicate electromigration are observed.

4.3.1.1 "Nuggets" and "holes"

Figure 25 shows an exemplary SEM images of AuCr after electrical testing ($J = 0.67$ MA/cm², $t = 6.3$ h, $\varepsilon = 15$ %, stripe geometry, survived). The contact area where one contact needle is attached to the sample surface can be seen and is indicated in the image (green circle). A ring of "holes" has formed around the contact. The ring is spread out toward the direction of the second contact. Inside this ring particles ("nuggets") can be found close to the contact. The red arrow marks the technical current direction from + to -, the yellow arrow symbolises the movement of the electrons in the opposite direction. Analysis of the phase diagram Au-Cr [38] shows that in the present temperature regime no phase transition occurs that could explain the occurrence of "holes" and "nuggets" as intermetallic phases.

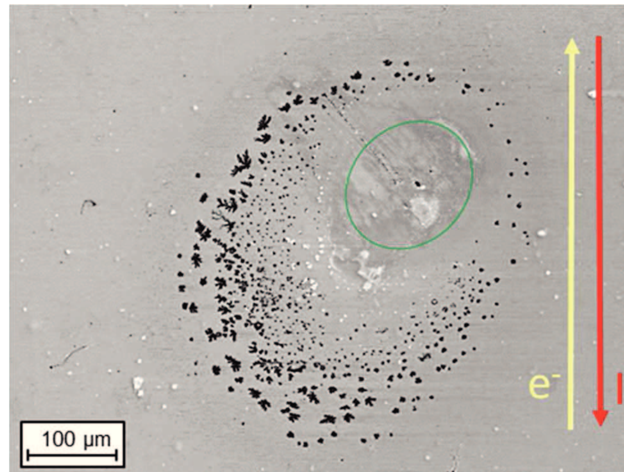

***Figure 25**: SEM micrograph of AuCr contact area, J = 0.67 MA/cm², t = 6.3 h. A ring of holes around and Au nuggets close to the contact evolved during electrical testing. The technical and physical current directions are indicated with red and yellow arrows respectively, the green circle indicates the position of one contact needle.*

EDS analysis was carried out to determine the chemical composition of the holes and nuggets (Figure 26). Spot scans reveal that the "nuggets" close to the contact consist of gold whereas particles outside of ring of holes are contaminations from the paste or atmosphere. Figure 26 (c) shows an exemplary SEM image of one "nugget". The EDS spot is marked with a cross and indicates that the nugget is Au.

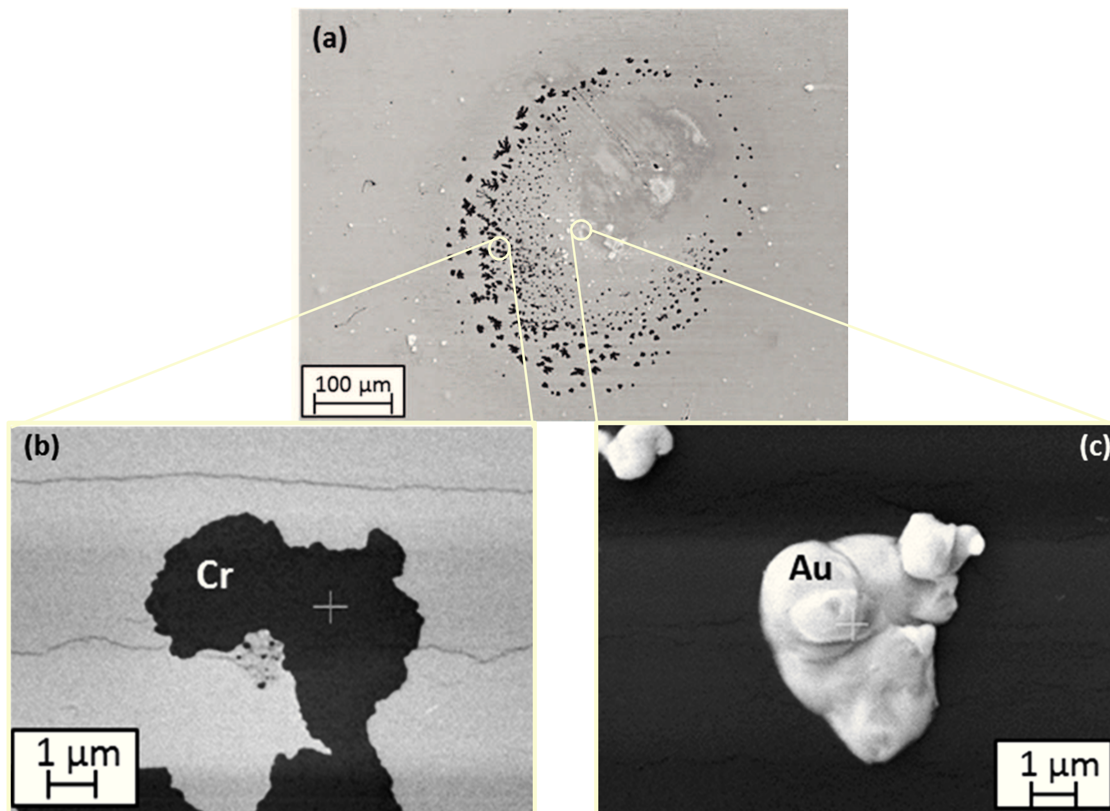

Figure 26*: EDS analysis of "nuggets and "holes" (a) overview, (b) hole, the Au top layer is missing in the dark region, (c) Au nugget.*

Figure 26 (b) shows a magnified SEM image of a hole. The corresponding EDS spectrum can be seen in Figure 27. Again the scanned spot is marked with a cross. The scan shows gold and chromium peaks and peaks at very low energies from light elements such as carbon. Reference scans of unobtrusive surfaces (without holes) were made for comparison. Most remarkable are the very strong peaks of light elements in hole-areas which increase with increasing amount of holes and cannot be found at intact surface areas. It is suggested, that those peaks stem from the absence of the gold layer in the whole regions. Gold as a heavy element absorbs parts of the low energetic X-ray radiation of light elements underneath. Missing of the Au layer can therefore explain the occurrence of low energy peaks from

lighter elements of the polymer substrate. Since Au is heavier than Cr, the 10 nm Cr interlayer can be neglected in absorption considerations.

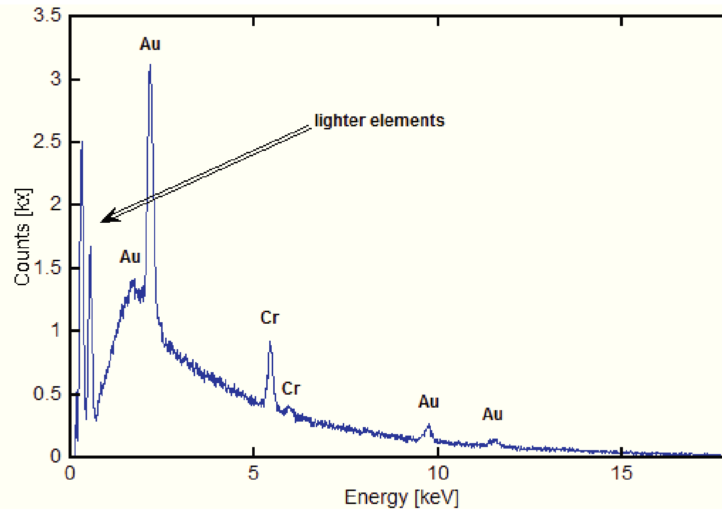

Figure 27*: EDS spectrum of a hole. Most remarkable are the peaks at very low energies that stem from lighter elements of the polyimide matrix. They are missing in the spectrum of intact surfaces and therefore indicate missing of the gold layer.*

The assumption that electromigration is observed results from the above mentioned phenomena. Gold particles which are missing in the holes move in the direction of the electrons and form nuggets closer to the contact. In the stripe geometry the local current density is highest at or close to the contacts due to flow line distribution. The local current density at the contacts can therefore exceed the calculated average of < 1 MA/cm². This circumstance justifies the occurrence of electromigration close to the contact for the stripe geometry.

AFM investigations were carried out to determine the topography of the holes. The images prove the idea of the missing gold layer. Figure 28 shows an exemplary AFM image of a hole and a height profile extracted from the image. The position of the extracted profile and the direction of the x-axis are marked with white lines.

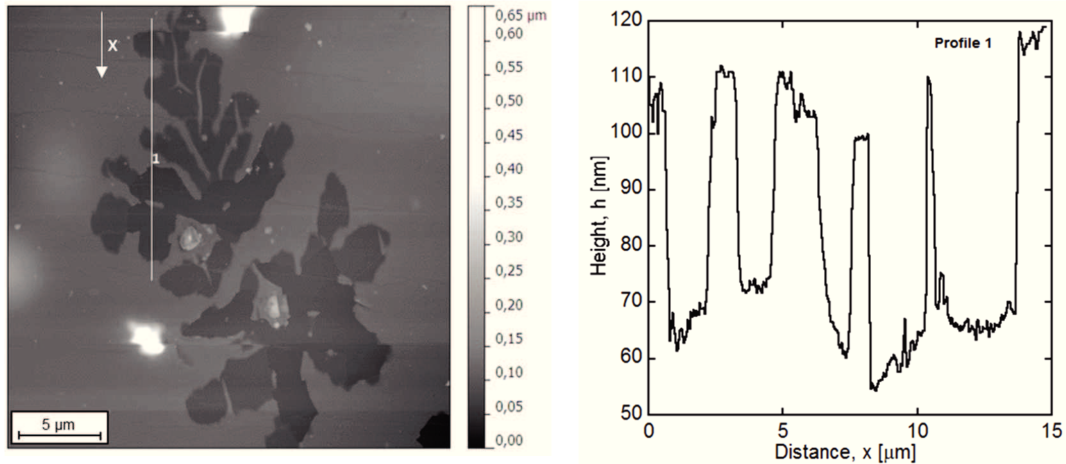

***Figure 28**: AFM height image of a hole (left) and extracted height profile (right). The position of the extracted profile is indicated with a white line. The dark areas in the AFM image have a mean depth of 40 nm.*

The height scale indicates that dark areas in the AFM image are deeper than areas with a brighter colour. The extracted height profile reveals, that the mean depth of the holes is between 40 and 50 nm. This implies that parts of the 50 nm top gold layer are missing in the dark hole-regions and that electromigration occurred.

4.3.1.2 Surface features

To visualize the influence of high current densities on cracks, SEM images of strained AuCr samples were taken before and after electrical testing. The examined area is located between two artificial cuts. Comparison of surface characteristics enables recognition of the same area before and after electrical testing. Figure 29 shows exemplary SEM images of AuCr before and after testing (J = 0.59 MA/cm², t = 24 h). The sample survived and the experiment was stopped after 24 hours. No clear statement can be made about the influence of high current densities on the cracks and a uniform change in the crack geometry is not obtained during testing. Cracks are still present after electrical testing.

Figure 29 (a) and (b) show that in some regions present cracks are more closed after electrical treatment than prior to testing. Other images falsify that assumption (Figure 29 (c) and (d)). Figure 29 (f) shows a magnification of Figure 29 (b) to give a better idea of the crack geometry after electrical testing. In this case, before and after images do not show the exact same area. After testing deformations oriented perpendicular to the original cracks are found on the surface. They form during testing between two TTCs due to thermal expansion and resulting thermal strains.

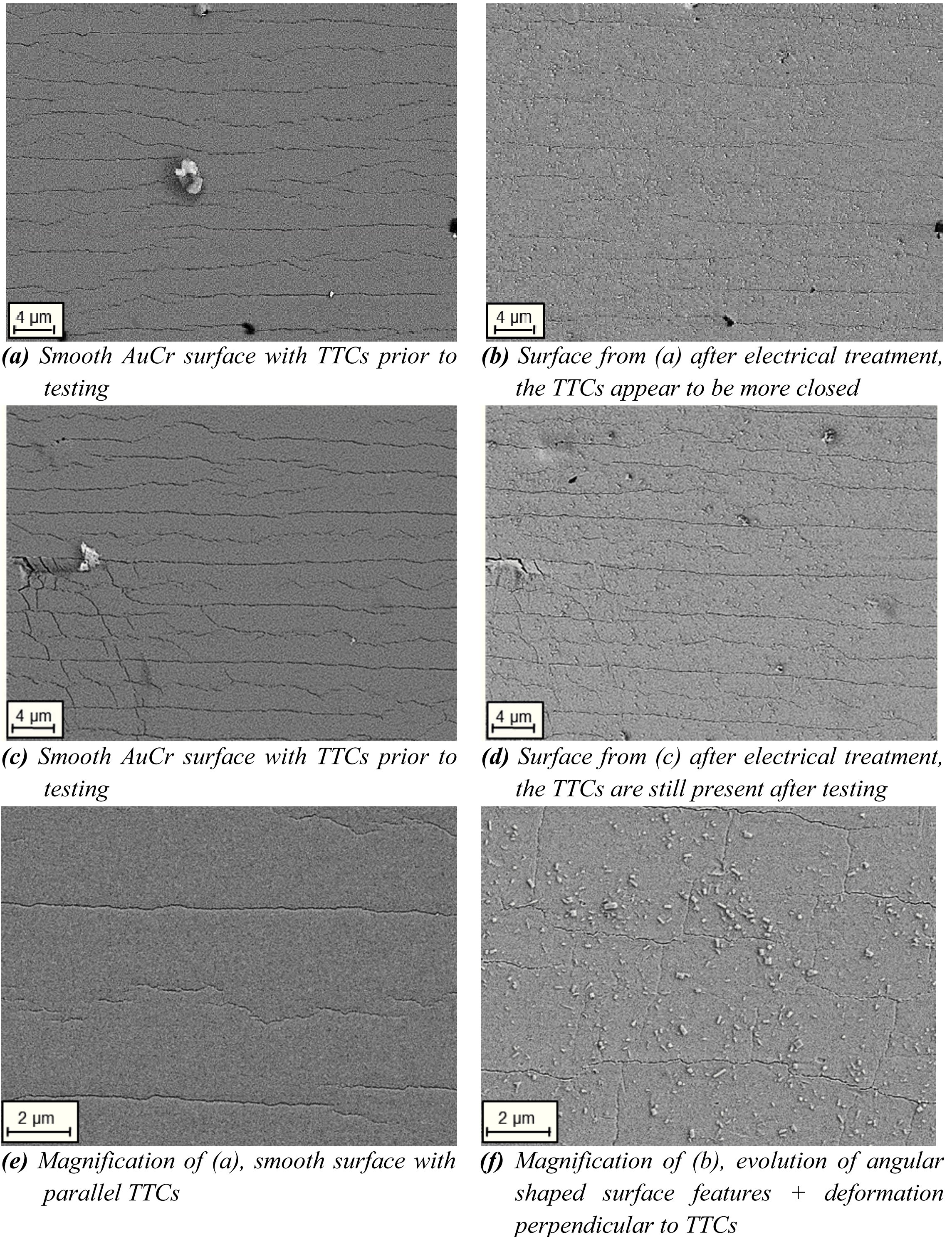

(a) *Smooth AuCr surface with TTCs prior to testing*

(b) *Surface from (a) after electrical treatment, the TTCs appear to be more closed*

(c) *Smooth AuCr surface with TTCs prior to testing*

(d) *Surface from (c) after electrical treatment, the TTCs are still present after testing*

(e) *Magnification of (a), smooth surface with parallel TTCs*

(f) *Magnification of (b), evolution of angular shaped surface features + deformation perpendicular to TTCs*

Figure 29*: SEM images prior to (a, c, e) and after (b, d, f) electrical testing, J = 0.59 MA/cm², t = 24 h, (a-b) and (c-d) show exact same area between two artificial cuts, (e-f) are from slightly different positions, surface roughening and the evolution of surface features can be seen after electrical treatment.*

Clearly observed is the formation of surface features during electrical treatment in both Au and AuCr. Prior to testing cracks are present but the surface is smooth. The roughening of the sample surface during testing can be seen in Figure 29. The surface features are angular shaped and in the magnitude of a few nm. They form between the cuts in the area with the highest current density and only in the area with the highest current density. It is suggested that the surface features are gold particles which formed during electrical testing due to electromigration. The features can be found only between the cracks in the region where the highest current density is present. EDS scans of the surface features need to be carried out to determine their chemical composition.

In Figure 30 the recorded normalised resistance curve over time of the above presented sample can be seen. The roughness of the curve (red mark) could indicate the formation of the surface features [30]. The peak at ~ 7 h is due to manual alteration of the current density and has no relevance.

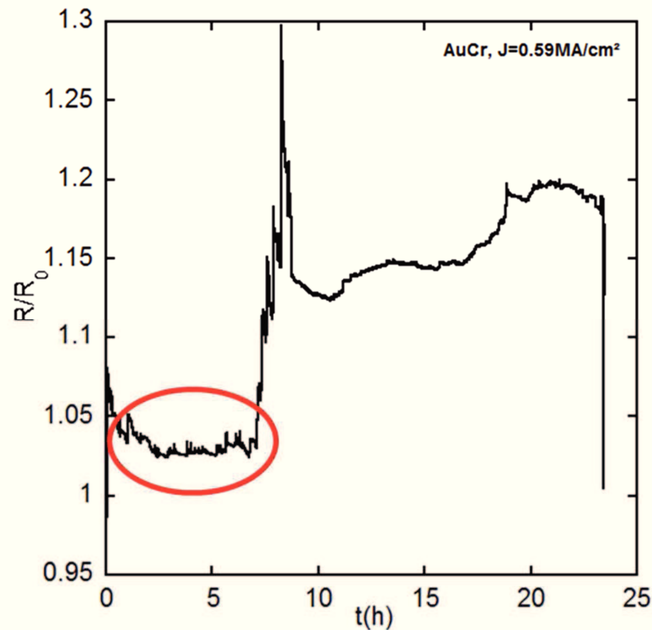

Figure 30*: Normalized resistance over time recorded for the sample presented in Figure 29. The very rough curve (red circle) can be related to the formation of surface features.*

Figure 31 (b) shows a SEM micrograph of Au after electrical testing (J = 1.36 MA/cm², t = 7 days). The evolution of surface features can be seen. For comparison Figure 31 (a) shows an image of a smooth surface in an untested region of the same sample.

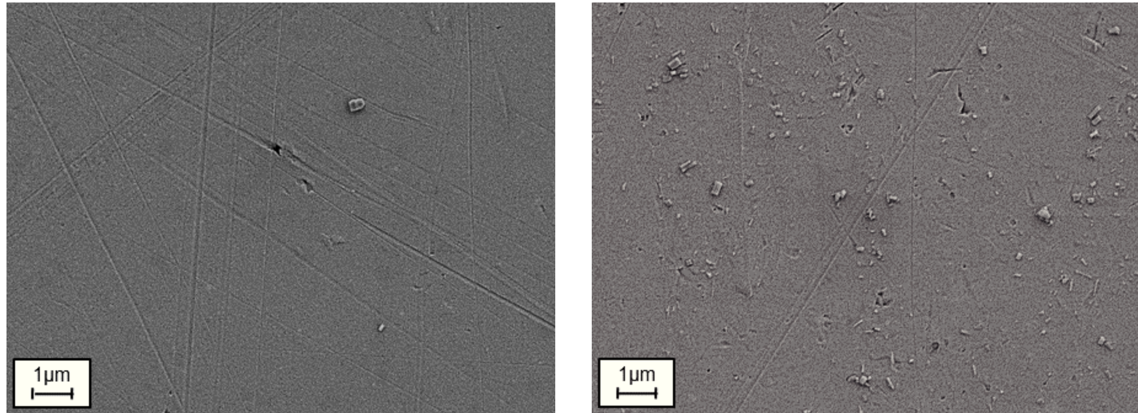

(a) *Smooth Au surface prior to electrical testing* ***(b)*** *Au surface after electrical testing (J = 1.36 MA/cm², t = 7 days), Evolution of surface features*

Figure 31*:Evoltuion of surface features in Au during electrical testing*

4.3.1.3 Long term failure

Electromigration also gives a second explanation about the long term failure of samples at contacts or in-between the cuts. Arising voids can consolidate leading to a locally increased current density and a temperature increase which induces a degradation of the polymer substrate. Unfortunately no revealing analysis of the metal surface is possible once the polymer matrix fails (compare failed samples Figure 21 and 22).

The above mentioned electromigration phenomena are obtained at current densities below the literature limit of J = 1 MA/cm². It has been mentioned before that the local current density can be higher than the calculated average value (flow line distribution, varying sample geometry, film thickness and inhomogeneities). In very thin films the limit value for J can be below 1 MA/cm². Small grain sizes enhance diffusion along grain boundaries. Diffusion processes along surfaces and interfaces can also reduce the current density limit and become more pronounced with decreasing film thickness [5].

5 Summary and Outlook

5.1 Electro-mechanical properties of Au and AuCr on PI

A 10 nm Cr interlayer causes brittle behaviour of a normally ductile 50 nm Au film. There is a good correlation between the ex-situ fragmentation tests and the in-situ electromechanical test (in-situ 4PP). In both cases the Au films with Cr interlayer show a brittle behaviour, forming TTCs perpendicular to the straining direction. Figure 32 shows a comparison of the mechanical and the electromechanical data for AuCr. The deviation from the theoretical line in the in-situ 4PP experiment corresponds with the cracking onset in fragmentation testing. The blue line in Figure 32 is plotted to guide the eye and has no scientific relevance. The fracture strain of AuCr is approximately $\varepsilon_f = 2$ %. After initial fracture saturation sets in very early at a strain of $\varepsilon_s \sim 4$ % according to fragmentation data. The average saturation crack spacing can be estimated with $\lambda_s \sim 5$ µm from AFM and SEM data.

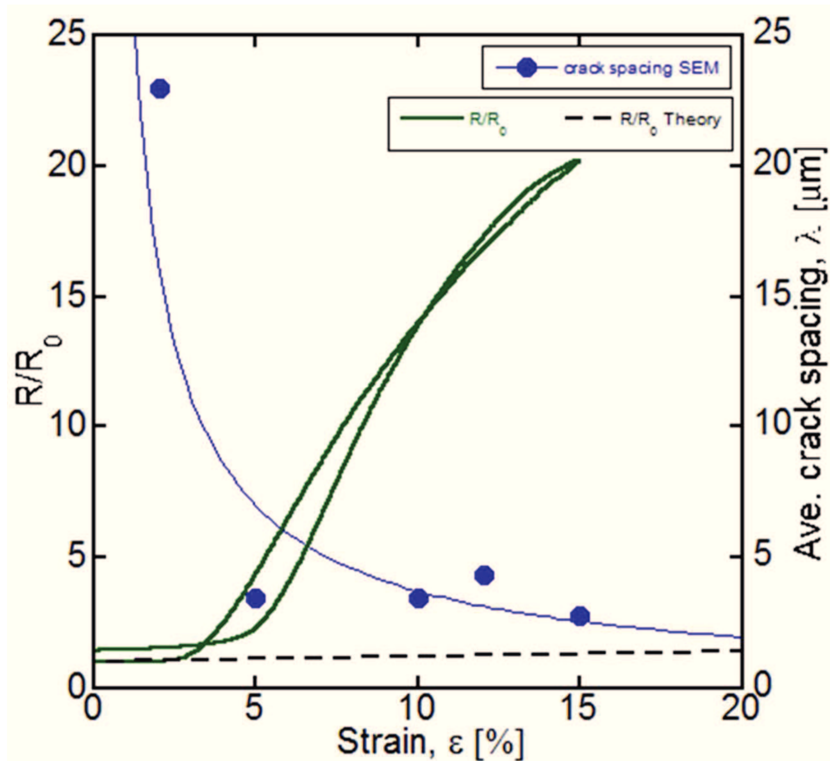

Figure 32: Comparison of in-site 4PP and ex-situ fragmentation test for AuCr. There is a good correlation between the results. The deviation of the resistance from the theoretical line (dotted black line) correlates with the fracture onset in the fragmentation test.

50 nm Au films without Cr interlayer show a ductile behaviour in uniaxial tension. The film resistance follows the theoretical line during straining and increases only because of elastic deformation of the sample. No evidence of cracking or deformation is observed and further fragmentation testing was not performed.

AFM and SEM imaging of the sample surfaces after testing confirms the brittle and ductile electro-mechanical behaviour of AuCr and Au respectively. The 10 nm Cr interlayer could improve adhesion between the film and the polymer because there is no evidence of delamination (e.g. buckles). However, further investigation of the 50 nm Au film using TEM is needed to fully understand its outstanding electro-mechanical behavior.

5.2 Electrical stability of Au and AuCr on PI; Electromigration

The influence of high current density on the electrical stability of Au and AuCr is investigated in this work. Thin gold films without Cr interlayer can endure higher current densities that those with Cr interlayer. Uncracked AuCr films allow for higher current densities than strained ones with TTCs perpendicular to the direction of the applied current. TTCs increase the probability of failure. No clear statement can be made about the influence of the electrical treatment on the crack geometry.

Failure occurs due to local melting of the polymer substrate. The time to failure scatters from immediate melting to long-term failure after various time frames depending on the magnitude of the current density. Locally increased current densities due to electromigration and changing microstructure of the metal film (evolution of pores and hillock) can explain long-term failure. Unfortunately no revealing analysis of the metal surface is possible once the polymer matrix fails. SEM imaging of the sample surfaces after electrical testing revealed two phenomena that indicate electromigration, namely the evolution of Au “nuggets” and “holes” and the evolution of surfaces features. The effects are obtained during electrical testing in both film systems. EDS and AFM analysis revealed the chemical composition and topography of Au nuggets and holes respectively. In the holes the Au top-layer is missing. The very rough shape of the resistance curve recorded at a constant testing current density can be related to the formation of surface features. Further EDS analysis need to be carried out to determine their chemical composition. The effects are obtained at current densities below the literature limit of 1 MA/cm² [4, 5]. In very thin films the limit value can be lower

due to increased diffusiveness. The microstructure contains a large number of rapid low-temperature diffusion paths, such as grain boundaries or interfaces [5].

One of the main challenges of this work is to generate high current densities in the gold films because of the relatively low thermal stability and local melting of the polymer matrix. For the electrical measurements a custom-made test configuration is used. Two contact needles force a constant current through a sample while the resistance is recorded. By successive improvements of the set-up, namely applying of the Cu-plate and thermal paste, optimisation of the contact needle distance and sample geometry, higher current densities in the metal films can be achieved over longer time frames compared to pre-trials.

The set-up is very sensitive to changes of the testing conditions (i.e. changes in room temperature or amount and propagation of the thermal paste due to temperature increase and softening of the paste). Further improvements such as a more effective cooling system or in-situ SEM experiments can help to create a less sensitive experimental set-up allowing for higher current densities.

Decreasing the sample dimensions down to a µm or nm scale and changing the geometry from stripe or cut geometry to a line geometry will result in an easier controllable electromigration test. With smaller dimensions lower currents are needed to generate high current densities and the effect of Joule Heating ($P=R*I^2$) diminishes. Furthermore optical detection of electromigration effects is facilitated with smaller samples since the area of interest is narrower. Intact and uncracked surfaces are favourable to detect electromigration phenomena with optical imaging. A plane and smooth sample surface makes it easier to identify potential pores and hillocks evolved during electrical treatment than a rough surface with a high initial defect density. Additionally small sample dimensions are closer to in use conditions in flexible electronics.

Electrical in-situ SEM experiments can reveal the direct coherence between alterations of the recorded resistance and electromigrative changes in microstructure such the evolution of pores and hillocks [30]. With the current testing configuration observation of the recorded resistance alteration does not really give information about potential electromigration effects. The setup is too sensitive to the environment to distinguish between microstructural changes and changes in the testing conditions. Preservation of completely constant conditions during testing is also not possible with the current setup. A primary requirement for

electrical in-situ SEM experiments is that the whole area of interest can be imaged during testing with a magnification, sufficiently high enough to detect the evolution of pores and hillocks (→ very small sample dimensions).

Testing at defined elevated temperatures can help to promote electromigration and obtain effects at lower current densities or shorter time frames. The limiting factor here is the thermal stability of the polymer substrate. The positive effect of high temperatures on the electromigrative diffusion process is explained in detail in the theoretical chapter about electromigration.

Applying high current densities to samples not only after but also during constant or altering mechanical loading (in-situ 4PP experiment with high applied current densities) can help to simulate stretching of a flexible electronic device in use and determine the influence of electrical straining on the mechanical fatigue.

I List of abbreviations

α	thermal coefficient of resistance
δ	thickness
Δ	depth
ε	strain
ε_s	saturation strain
ε_f	fracture strain
λ	crack spacing
λ_s	saturation crack spacing
ρ	resistivity
ρ_B	bulk resistivity
σf	failure stress
$\Delta\sigma$	maximum stress
$\delta\sigma/\delta x$	stress gradient
τ_{max}	maximum shear stress
Ω	atomic volume
A	cross-section
A_0	initial cross-section
AFM	atomic force microscope
Ag	silver
Au	gold
AuCr	gold film with chromium interlayer
B	empirical constant
bcc	body centered cubic
BSE	backscattered electrons
C	concentration of atoms
Cr	chromium
Cu	copper
D	diffusion coefficient
D_0	maximum diffusion coefficient at infinite temperature

DC	direct current
e	fundamental electronic charge
E	electric field
E_a	activation energy
EDS	energy dispersive X-ray analysis
Eq.	Equation
F	force
fcc	face centered cubic
4PP	four point probe
h	height
I	current
ITO	indium tin oxide
J	current density
J_a	atomic flux
J_c	threshold current density
$(JL)_c$	critical product
k	Boltzmann's constant
K	numerical constant
L	length
L_o	initial length
ΔL	length difference
L_{th}	Blech Length
n	current density exponent
Ni	nickel
P	heat
PC	polycarbonate
PE	polyester
PE DOT:PSS	Poly (3,4-ethylenedioxythiophene) poly (styrenesulfonate)
PET	polyethyleneterephthate
PI	polyimide
PVD	physical vapour deposition

R	resistance
R_0	initial resistance
R_{End}	final resistance
R_{meas}	total measured resistance
R_{samp}	resistance of strained part of the sample
R_{const}	constant contact resistance
R/R_0	normalised resistance
$R/R_{0\,max}$	maximum normalised resistance
$R/R_{0\,End}$	final normalised resistance
SE	secondary electrons
SEM	scanning electron microscope
t	time
t_{50}	median time to failure
T	temperature
T_0	initial temperature
T_m	melting temperature
T_s	temperature of thermal stability
ΔT	temperature difference
Ta	tantalum
TEM	transmission electron microscopy
Ti	titanium
TiN	titanium nitride
TTC	Through Thickness Crack
V	voltage
w	width
W	tungsten
x	Distance
XRD	X-ray diffraction
v_D	drift velocity
Z*	effective charge number

II List of figures

Figure 1: Schematic of an evaporation process. The metal, which is to be deposited, is evaporated from a source using thermal energy and condenses on the substrate surface forming a film [10]. .... - 5 -

Figure 2: Schematic of a sputter process. Atoms are ejected from a metal target through collisions with incident plasma-ions and deposited onto a substrate surface forming a film [10]. .... - 5 -

Figure 3: Failure of a ductile metal film, (a) free-standing and (b) on polymer substrate, (c) delamination [3].. - 7 -

Figure 4: Failure of a brittle film, (a) free standing and (b) on polymer substrate [12]. . - 8 -

Figure 5: Fragmentation Test of a brittle metal film. The average crack spacing measured with AFM and SEM is plotted over the applied strain. The plateau indicates saturation. SEM and AFM results follow one another closely [19]. .... - 10 -

Figure 6: Fragmentation Test of a ductile metal film. The average deformation spacing measured with AFM and SEM is plotted over the applied strain. The plateau indicates saturation. SEM and AFM results differ from each other, especially at small applied strains [19]. .... - 10 -

Figure 7: Exemplary curves derived in an in-situ 4PP experiment: (a) Engineering stress vs. realtive elongation, (b) Relative resistances R/R_0 vs. relative elongation. R_{meas}/R_{0meas} and R_{samp}/R_{0amp} equal the measured and corrected relative resistance respectively. The solid square shows the corrected relative resistance recorded 24 h after tensile testing and indicates relaxation processes. Eq. (4) represents the theoretical line for elastic deformation. Eq. (3) can be neglected [6]. .... - 12 -

Figure 8: Schematic setup of the drift test. Metal stripes (Al) of various lengths are patterned onto a conductive Titanium Nitride (TiN) film. The current shunts through the lower-resistance Al stripes [30]. .... - 17 -

Figure 9: Single stripe undergoing electromigration. Voids and hillocks evolve at the anode and cathode respectively [10]. .... - 17 -

Figure 10: Drift test conducted on aluminium (J=3.7*10^5 A/cm²). The effect of electromigration increases with increasing stripe length. The shortest stripe (left) has a subcritical length and shows no damage [10].. - 18 -

Figure 11: Schematics of the investigated film-substrate systems, AuCr: 50 nm Au film sputter deposited onto a 50 µm polyimide substrate. A 10 nm Cr interlayer is used to improve adhesion; Au: 50 nm Au film sputter deposited onto a 50 µm polyimide substrate, no adhesion layer. .... - 20 -

Figure 12: (a) Experimental setup of in-situ 4PP experiment and image of mounted sample [6]. The resistance of a thin film is recorded during uniaxial loading and unloading of the sample. (b) 4 point probe setup for reference measurement of R_0 to determine R_{const}... - 23 -

Figure 13: Experimental setup for electrical testing. A constant current is forced through the film while the resulting voltage is sensed. The film resistance is calculated using Ohm's law and recorded over time. .... - 24 -

Figure 14: Different sample geometries used for electrical testing: (a) stripe geometry: constant current density over the cross section; (b) cut geometry: artificial cuts on both sides locally increase the current density and narrow the area of interest............................. - 24 -

Figure 15: (a) AFM height image at 15 % strain of AuCr film. The positions of the extracted surface profiles and the straining direction are indicated. (b) Surface profile from (a) indicating where TTCs have formed (Black arrows). The distance λ is the measured crack spacing between two TTCs. .... - 25 -

Figure 16: SEM micrograph at 15% strain of AuCr. Black arrows indicate TTCs. The distance λ equals the measured crack spacing between two TTCs. The straining direction is indicated on the right side of the image.. - 26 -

Figure 17: Average crack spacing evolution of AuCr as a function of strain. The crack spacing is measured with AFM and SEM. The standard deviation is depicted with error bars. The results follow one another closely. The plateau indicates saturation. Saturation spacing can be estimated with $\lambda_s \sim 5$ µm. .... - 27 -

Figure 18: Change of the normalized electrical resistance R/R_0 with increasing normalized length L/L_0 during straining of Au and AuCr, ε_{max}=15 %. The curves show the calculated average of four tested samples for each system. Error bars depict the standard deviation at representative points. The obtained behaviours strongly differ from each other. .... - 28 -

Figure 19: AFM images of the sample surface after electromechanical testing, ε=15 %,straining direction is indicated, (a) AuCr, TTCs perpendicular to straining direction can be seen, (b) Au, no evidence for localized thinning (necking) or TTCs perpendicular to straining direction. The features parallel to straining direction stem from deposition and elongate during straining. .... - 30 -

Figure 20: Map of electrical treatments, Au and AuCr samples are exposed to different current densities over various time frames. Above 1.5 MA/cm² all samples fail, below that value the samples ether survive the treatment or fail after a certain time. For surviving samples experiments are stopped after a maximum of 7 days if no significant change in the recorded resistance is obtained. .... - 31 -

Figure 21: Failed and survived samples of AuCr, strained and unstrained. Failure occurs in form of local decomposition of the polymer substrate. Microstructural changes occur preferentially at the cut tips. Long term failure can be explained by electromigrative change of the microstructure (see Chapter 4.3.1.3). .... - 32 -

Figure 22: Failed and survived samples, Au, all unstrained. Failure occurs in form of local decomposition of the polymer substrate. Microstructural changes occur preferentially at the cut tips. Long term failure can be explained by electromigrative change of the microstructure (see Chapter 4.3.1.3). .... - 34 -

Figure 23: Initialisation phase of the electrical testing, the red circle marks the region were the critical limit of the current density is exceeded (rapid increase of R/R_0), subsequently the current density was decreased and the testing was performed at a lower value............ - 36 -

Figure 24: Normalised resistance over time for Au and AuCr, strained and unstrained, all cut-geometry. The curves do not differ significantly from each other. The experiments were stopped after 5 and 7 days. Variation of the recorded resistance can be evidence of electromigration or changing testing conditions. The jumps in the orange and blue curve stem for manual manipulation and can be neglected.. - 38 -

Figure 25: SEM micrograph of AuCr contact area, J = 0.67 MA/cm², t = 6.3 h. A ring of holes around and Au nuggets close to the contact evolved during electrical testing. The technical and physical current directions are indicated with red and yellow arrows respectively, the green circle indicates the position of one contact needle. .... - 39 -

Figure 26: EDS analysis of “nuggets and “holes” (a) overview, (b) hole, the Au top layer is missing in the dark region, (c) Au nugget. .... - 40 -
Figure 27: EDS spectrum of a hole. Most remarkable are the peaks at very low energies that stem from lighter elements of the polyimide matrix. They are missing in the spectrum of intact surfaces and therefore indicate missing of the gold layer.................................... - 41 -
Figure 28: AFM height image of a hole (left) and extracted height profile (right). The position of the extracted profile is indicated with a white line. The dark areas in the AFM image have a mean depth of 40 nm. .... - 42 -
Figure 29: SEM images prior to (a, c, e) and after (b, d, f) electrical testing, J = 0.59 MA/cm², t = 24 h, (a-b) and (c-d) show exact same area between two artificial cuts, (e-f) are from slightly different positions, surface roughening and the evolution of surface features can be seen after electrical treatment. .... - 43 -
Figure 30: Normalized resistance over time recorded for the sample presented in Figure 29. The very rough curve (red circle) can be related to the formation of surface features. . - 44 -
Figure 31:Evoltuion of surface features in Au during electrical testing....................... - 45 -
Figure 32: Comparison of in-site 4PP and ex-situ fragmentation test for AuCr. There is a good correlation between the results. The deviation from the theoretical line (dotted black line) correlates with the fracture onset in the fragmentation test. .... - 46 -

III List of tables

Table 1: Overview of relevant material characteristics and functions of the different layers of the film-substrate system - 21 -

Table 2: Summary of characteristic data of Au and AuCr from Figure 18 - 28 -

IV References

[1] S. Béfahy, Stretchable helical gold conductor on silicone rubber microwire.

[2] N. Lambricht, T. Pardoen, S. Yunus, Giant stretchability of thin gold films on rough elastomeric substrates, Acta Materialia 61, 2013, 540–547.

[3] M. J. Cordill, Flexible Film Systems: Current Understanding and Future Prospects, JOM, Vol. 62, No. 6.

[4] B. Valek, J.C. Bravman, N. Tamura, A.A. MacDowell, R.S. Celestre, H.A. Padmore, R. Spolenak, W.L. Brown, B.W. Batterman, J. R. Patel, Electromigration-induced plastic deformation in passivated metal lines, Applied Physics Letters, Volume 81, No. 22, 2002.

[5] J. R. Lloyd, Electromigration in integrated circuit conductors, J. Phxs. D: Appl. Phys. 32, 1999, R109-R118.

[6] O. Glushko, M. J.Cordill, Electrical resistance of metal films on polymer substrated under tension, Experimental Techniques. doi: 10.1111/ext.12082, 2014.

[7] W. D. Nix, Mechanical properties of thin films, Metallurgical Transactions A, November 1989, Volume 20, Issue 11, pp 2217-2245.

[8] M. Ohring, Material Science of Thin Films, Academic Press, 2002, p 95-273.

[9] E. Sacher, Jean-Jacques Pireaux, Steven P. Kowalczyk, Metallization of Polymers, American Chemical Society, 1990, xiv, 528 p..

[10] L. Freund, S. Suresh, Thin Film Materials, Cambridge University Press, 2003, p 697-711.

[11] T. Li, Z. Suo, Ductility of thin metal films on polymer substrates modulated by interfacial adhesion, International Journal of Solids and Structures 44, 2007, 1696-1705.

[12] T. Li, Z. Y. Huang, Z.C. Xi, S.P.Lacour, S. Wagner, Z. Suo, Delocalizing strain in a thin metal film on polymer substrate, Mechanics of Materials 37, 2005, 261-273.

[13] J. D. Yeager, Derrick J. Phillips , David M. Rector, David F. Bahr, Characterization of flexible ECoG electrode arrays for chronic recording in awake rats, Journal of Neuroscience Methods 173, 2008, 279–285.

[14] A. A. Taylor, Megan Jo Cordill, Gerhard Dehm, On the limits of the interfacial yield model for fragmentation testing of brittle films on polymer substrates, Philosophical Magazine, 2012, DOI:10.1080/14786435.2012.723145.

[15] T. Lacroix, R. Keunings, M. Desaeger, I. Verpoest, A new data reduction scheme for the fragmentation testing of polymer composites, Journal of Material Science 30, 1995, 683-692.

[16] T. Lacroix, B. Tilmans, R. Keunings, M. Desaeger, I. Verpoest, Modelling of critical fibre length and interfacial debonding in the fragmentation testing of polymer composites, Composite Science and Technology 43, 1992, 379-387.

[17] A.A. Taylor, V. Edlmayr, M.J. Cordill, G. Dehm, The effect of film thickness variations in periodic cracking: Analysis and experiments, Surface & Coatings Technology 206, 2011, 1830–1836.

[18] A. Taylor, V. Edlmayr, M.J. Cordill, G. Dehm, The effect of temperature and strain rate on the periodic cracking of amorphous AlxOy films on Cu, Surface & Coatings Technology 206, 2011, 1855–1859.

[19] M. Cordill, V.M. Marx, Fragmentation testing for ductile thin films on polymer substrates, Philosophical Magazine Letters 93/11, 2013, 618-624.

[20] F. Toth, F. G. Rammerstorfer, M.J. Cordill, F.D Fischer, Detailed Modelling of Delamination Buckling of Thin Films Under Global Tension, Acta Materialia 61, 2013, 2425-2433.

[21] J. Andersons, S. Tarasovs, Y. Leterrier, Evaluation of thin film adhesion to a compliant substrate by the analysis of progressive buckling in the fragmentation test, Thin Solid Films 517, 2009, 2007-2011.

[22] M. Cordill, F.D. Fischer, F.G. Rammerstorfer, G. Dehm, Adhesion energies of Cr thin films on polyimide determined from buckling: Experiment and model,Acta Materialia 58, 2010, 5520–5531.

[23] T. Li, Zhenyu Huand, Z Suo, Stephanie P Lacour, Sigurd Wagner, Stretchability of thin metal films on elastomer substrates, Applied Physics Letters, V. 85, No. 16, 2004.

[24] O. Glushko, V.M.Marx, C. Kirchlechner, I. Zizak, M.J. Cordill, Recovery of electrical resistance in copper films on polyethylene terephthalate subjected to a tensile strain, Thin Solid Films 552, 2014, 141–145.

[25] S. Kasap, Principles of Electrical Engineering Materials and Devices, McGraw-Hill Higher Education, 2000, p. 141-143.

[26] http://lima.osu.edu/academics/physics/103/LectureSlides/Period13SlidesHandouts.pdf, 04.02.2014.

[27] http://hyperphysics.phy-astr.gsu.edu/hbase/electric/restmp.html, 04.02.2014.

[28] C. S. Hau-Riege, An introduction to Cu electromigration, Microelectronics Reliability 44, 2004, 195–205.

[29] X. Wang, Xianping Dong, Jiansheng Wu, Effects of Cr dopant on the microstructure and electromigration performance of Cu interconnects, Applied Surface Science 255, 2009, 9273-9278.

[30] B. Stahlmecke, Elektromigration in Gold und Silber Nanostrukturen, Fachbereich Physik der Universität Duisburg-Essen (Standort Duisburg), Dissertation, 2008.

[31] I. Blech, Electromigration in thin aluminum films on titanium nitride, Journal of Applied Physiys, Vol. 47, No. 4, April 1976.

[32] J. D. Yeager, David F. Bahr, Microstructural characterization of thin gold films on a polyimide substrate, Thin Solid Films 518, 2010, 5896–5900.

[33] http://www.engineeringtoolbox.com/resistivity-conductivity-d_418.html (07.04.2014).

[34] http://www.allaboutcircuits.com/vol_1/chpt_12/6.html, (07.04.2014).

[35] D. Neßas, Petr Klapetek, Gwyddion: an open-source software for SPM data analysis, Cent. Eur. J. Phys. 10(1), 2012, 181-188.

[36] M. Abramoff, Magalhaes, P.J., Ram, S.J. "Image Processing with ImageJ". Biophotonics International, volume 11, issue 7, pp. 36-42, 2004.

[37] N.-J. Wu, , S. Shimizu, M.T. Hermie, K. Sakamoto, A. Natori, H. Yasunaga, Surface electromigration of Au ultrathin film on MoS2, Applied Surface Science 169-170, 2001, 485-488.

[38] O. Madelung, Landolt-Börnstein - Group IV Physical Chemistry Volume 5a, 1991, pp 1-3.